Research Paper

GEOSPHERE

GEOSPHERE, v. 17, no. 1

https://doi.org/10.1130/GES02284.1

13 figures; 2 tables; 1 set of supplemental files

CORRESPONDENCE:
eschwarz@cig.museo.unlp.edu.ar

CITATION: Schwarz, E., Finzel, E.S., Veiga, G.D., Rapela, C.W., Echevarria, C., and Spalletti, L.A., 2021, U-Pb geochronology and paleogeography of the Valanginian–Hauterivian Neuquén Basin: Implications for Gondwana-scale source areas: Geosphere, v. 17, no. 1, p. 244–270, https://doi.org/10.1130/GES02284.1.

Science Editor: David E. Fastovsky
Associate Editor: Christopher Spencer

Received 12 May 2020
Revision received 2 August 2020
Accepted 20 November 2020

Published online 23 December 2020

U-Pb geochronology and paleogeography of the Valanginian–Hauterivian Neuquén Basin: Implications for Gondwana-scale source areas

E. Schwarz[1,*], E.S. Finzel[2,*], G.D. Veiga[1], C.W. Rapela[1], C. Echevarria[3,*], and L.A. Spalletti[1]

[1]Centro de Investigaciones Geológicas (Universidad Nacional de La Plata–Consejo Nacional de Investigaciones Científicas y Técnicas [CONICET]), Diagonal 113 #256 B1904DPK, La Plata, Argentina
[2]Earth and Environmental Science Department, University of Iowa, 115 Trowbridge Hall, Iowa City, Iowa 52242, USA
[3]Pampa Energía S.A. Gerencia Tight, Dirección de E&P, J.J. Lastra 6000, 8300 Neuquén, Argentina

ABSTRACT

Sedimentary basins located at the margins of continents act as the final base level for continental-scale catchments that are sometimes located thousands of kilometers away from the basin, and this condition of exceptionally long sediment transfer zones is probably reinforced in supercontinents, such as Gondwana. One of the most prominent marine basins in southwestern Gondwana during the Jurassic and Early Cretaceous was the Neuquén Basin (west-central Argentina), but its role as a sediment repository of far-flung source areas has not been extensively considered. This contribution provides the first detailed detrital-zircon U-Pb geochronology of the Valanginian–Hauterivian Pilmatué Member of the Agrio Formation, which is combined with sedimentology and paleogeographic reconstructions of the unit within the Neuquén Basin for a better understanding of the fluvial delivery systems. Our detrital-zircon signatures suggest that Triassic–Permian zircon populations were probably sourced from the adjacent western sector of the North Patagonian Massif, whereas Early Jurassic, Cambrian, Ordovician, and Proterozoic grains were most likely derived from farther east, in the eastern sector of the North Patagonian Massif, as well as presently remote terranes such as the Saldania Belt in southern Africa. We thus propose a Valanginian–Hauterivian longitudinal delivery system that, starting in the mid-continent region of southwestern Gondwana and by effective sorting, was bringing fine-grained or finer caliber sand to the Neuquén Basin shoreline. This delivery system was probably active (though not necessarily continuously) from Early Jurassic to Early Cretaceous until finally coming to an end during the opening of the South Atlantic Ocean in the latest Early Cretaceous.

Ernesto Schwarz https://orcid.org/0000-0002-8518-3728
*E-mails: eschwarz@cig.museo.unlp.edu.ar; emily-finzel@uiowa.edu; carlos.echevarria@pampaenergia.com

1. INTRODUCTION

The detailed reconstruction of long-lived sediment source areas for marine basins in deep time is commonly hampered by the fact that some, if not all, of the main sources could presently be far away from their previously linked marine repositories. In active tectonic basins, such as backarc basins, this can be even more difficult considering that depending upon their deformational style, these marine basins can receive sediment from the arc, adjacent cratonic areas, or even remote source areas located hundreds of kilometers from the coeval shoreline. Provenance studies based solely on sandstone petrography or heavy-mineral analyses typically identify the most proximal potential source areas as the primary sources because compositional data have less precision in identifying source areas so the nearest match is often identified. In contrast, detrital-zircon U-Pb geochronology of basin strata often facilitates the identification of, and even requires, sediment flux from far-removed source areas.

One of the most prominent marine basins in southwestern Gondwana during the Jurassic and Early Cretaceous was the Neuquén Basin, which during that time was a backarc basin separated from the proto–Pacific Ocean (i.e., to the west) by a discontinuous volcanic arc (Howell et al., 2005). This marine basin was bounded by the Sierra Pintada–Las Matras–Chadileuvú blocks to the northeast and the North Patagonian Massif to the southeast. The relatively little data produced from detrital-zircon grains for the Jurassic and Early Cretaceous strata allowed previous authors to suggest a change in provenance from dominantly western (arc) sources in the Early and Late Jurassic, to an eastern-dominated (cratonic) source for the Early Cretaceous (Naipauer et al., 2014; Naipauer and Ramos, 2016). This apparent change, recorded in the Early Cretaceous strata (Agrio and Rayoso formations), was attributed to either a basin base-level fall or, alternatively, uplift and exhumation of the eastern foreland region (Naipauer et al., 2014; Naipauer and Ramos, 2016). The possibility of the Neuquén Basin as the sediment repository of remote source areas within Gondwana has not been considered.

This contribution provides the first detailed detrital-zircon U-Pb analysis of fluvial and deltaic sandstones of the Pilmatué Member of the Lower Cretaceous Agrio Formation (Neuquén Basin, Argentina); this analysis is combined with sedimentology, geochronology, and biostratigraphy to: (1) present detailed paleoenvironmental and paleogeographic reconstructions of the Pilmatué Member; (2) provide detailed analysis of the detrital-zircon age patterns and potential sediment source rocks; and (3) discuss the implications for far-flung versus nearby source areas for the Lower

Cretaceous strata of the Neuquén Basin in the context of southwestern Gondwana paleogeography.

2. GEOLOGIC AND STRATIGRAPHIC SETTING

The Neuquén Basin is a sedimentary depression located on the eastern side of the Andes in west-central Argentina, between latitudes 32° and 40° South (Fig. 1A). It covers an area of over 200,000 km^2 and is bounded by tectonically stable areas to the northeast (Sierra Pintada, Las Matras, and Chadileuvú blocks) and south and southeast (North Patagonian Massif) (Figs. 1A and 1B). The sedimentary record of the Neuquén Basin includes continental and marine siliciclastics, carbonates, and evaporites, which accumulated under a variety of basin styles between the Late Triassic to the early Cenozoic (Legarreta and Uliana, 1991; Howell et al., 2005).

During the Late Triassic to the earliest Early Jurassic, this western border of Gondwana was characterized by large transcurrent fault systems (Franzese and Spalletti, 2001). This led to extensional tectonics within the Neuquén Basin and the evolution of a series of narrow, relatively isolated depocenters (Franzese and Spalletti, 2001), which were mostly filled with volcanic and continental successions collectively termed the PreCuyo Group or Precuyano Cycle (Franzese et al., 2006; Carbone et al., 2011; Muravchik et al., 2011) (Fig. 2). Due to continuous subduction at the proto-Pacific margin of Gondwana, a transition from synrift to postrift conditions occurred in the late Early Jurassic (Vergani et al., 1995), marked by the first marine incursion in the basin. The Neuquén Basin became a backarc depocenter characterized for the most part by regional, slow subsidence (sag and/or postrift phase) that lasted to the end of the Early Cretaceous (Legarreta and Uliana, 1991). Despite the long-term sag phase, several shorter-term contractional phases occurred through the Middle Jurassic to Early Cretaceous (Fig. 2), producing inversion and exhumation of previous strata and readjustment of the depositional systems in the basin (Vergani et al., 1995; Howell et al., 2005).

In the earliest stages of the sag phase (Cuyo and Lotena groups, Lower-Middle Jurassic, Fig. 2), the marine basin developed steep gradients, and sediment gravity flows were common in distal sectors of the marine depositional systems (e.g., Burgess et al., 2000). A complete disconnection of the marine basin with the proto–Pacific Ocean occurred during the Late Jurassic (Tordillo Formation, Kimmeridgian), probably due to basin-wide tectonic uplift (Vergani et al., 1995). This triggered the development of widespread continental systems, from coarse alluvial deposits to eolian sediments (Spalletti and Veiga, 2007; Spalletti et al., 2011). The marine connection was re-established in Tithonian–Berriasian times and lasted to the middle Barremian (Fig. 2), but this new basin was characterized by a ramp-type profile along the eastern and southern margins (Howell et al., 2005; Schwarz et al., 2018b) with development of gentle slopes in some distal marine environments (e.g., the Vaca Muerta clinoforms, Dominguez and Di Benedetto, 2018). The Mendoza Group includes all the outcrop and subsurface marine to continental sedimentary strata developed during the Tithonian–Barremian period and can be separated into three depositional phases or sequences: the Vaca Muerta–Picún Leufú–Quintuco–Loma Montosa sequence, the Mulichinco-Pilmatué Member sequence, and the Avilé–Agrio de la Mula Member sequence (Fig. 2).

The late Barremian–early Aptian interval (Huitrín Formation, Fig. 2) is dominated by a drastic relative sea-level fall and the deposition of fluvial and eolian sediments in most of the basin, which was subsequently covered by shallow-marine waters resulting in the deposition of evaporites and carbonates, and the preservation of older eolian dunes (Veiga et al., 2005; Veiga and Vergani, 2011; Argüello Scotti and Veiga, 2018). The invertebrate macrofauna in the carbonates of the La Tosca Member suggest a restricted marine setting (Lazo and Damborenea, 2011), and therefore a partial connection of the Neuquén Basin with the proto–Pacific Ocean cannot be discarded. The overlying Rayoso Formation (Fig. 2) is composed of fluvial, lacustrine, and evaporite deposits that extend across the basin (Zavala et al., 2006; Zavala and Ponce, 2011). By the end of the Early Cretaceous, the deformational tectonic regime of southwestern Gondwana became contractional and recorded the first Andean uplift (Tunik et al., 2010). The Neuquén depocenter transitioned to a foreland basin with eastward migration of the orogenic front and accumulation of synorogenic deposits recorded in the Neuquén Group and equivalent units (Vergani et al., 1995; Cobbold and Rossello, 2003; Tunik et al., 2010). The connection with the proto–Pacific Ocean ceased and was followed by extensive continental deposition in the basin between the Late Cretaceous and the Paleogene (Fig. 2).

Over the past ten years, the geochronology of some stratigraphic units in the Neuquén Basin has been significantly improved based on absolute U-Pb ages from igneous basement rocks and Upper Triassic–Lower Jurassic synrift deposits (see Naipauer and Ramos, 2016, for a summary) (Fig. 2). Absolute ages (U-Pb thermal ionization mass spectrometry [TIMS] and sensitive high-resolution microprobe [SHIRMP]) are also available for tuffs interbedded in the Agrio Formation, helping to constrain the study interval (Aguirre-Urreta et al., 2015, 2017, 2019; Schwarz et al., 2016). Provenance studies that utilize detrital-zircon U-Pb geochronology and isotope (Hf) compositions have also received recent attention, and zircon age distributions from lithostratigraphic units in the synrift to foreland packages are published, although several of these studies are low n (n ~ 100); so the relative abundance of various age groups can be unreliable (Pullen et al., 2014; Fig. 2). Importantly, zircon age distributions from the Avilé Member, which overlies the Pilmatué Member in the Neuquén sector of the basin, were reported by Tunik et al. (2010).

2.1 Pilmatué Member Background

The Pilmatué Member of the Agrio Formation, originally termed Lower Agrio Member (Weaver, 1931), is a regionally extensive unit that can be stratigraphically identified from the western Neuquén Embayment to the entire Main Cordillera (Figs. 1C and 3A). Its base marks a significant deepening with respect to the underlying continental or

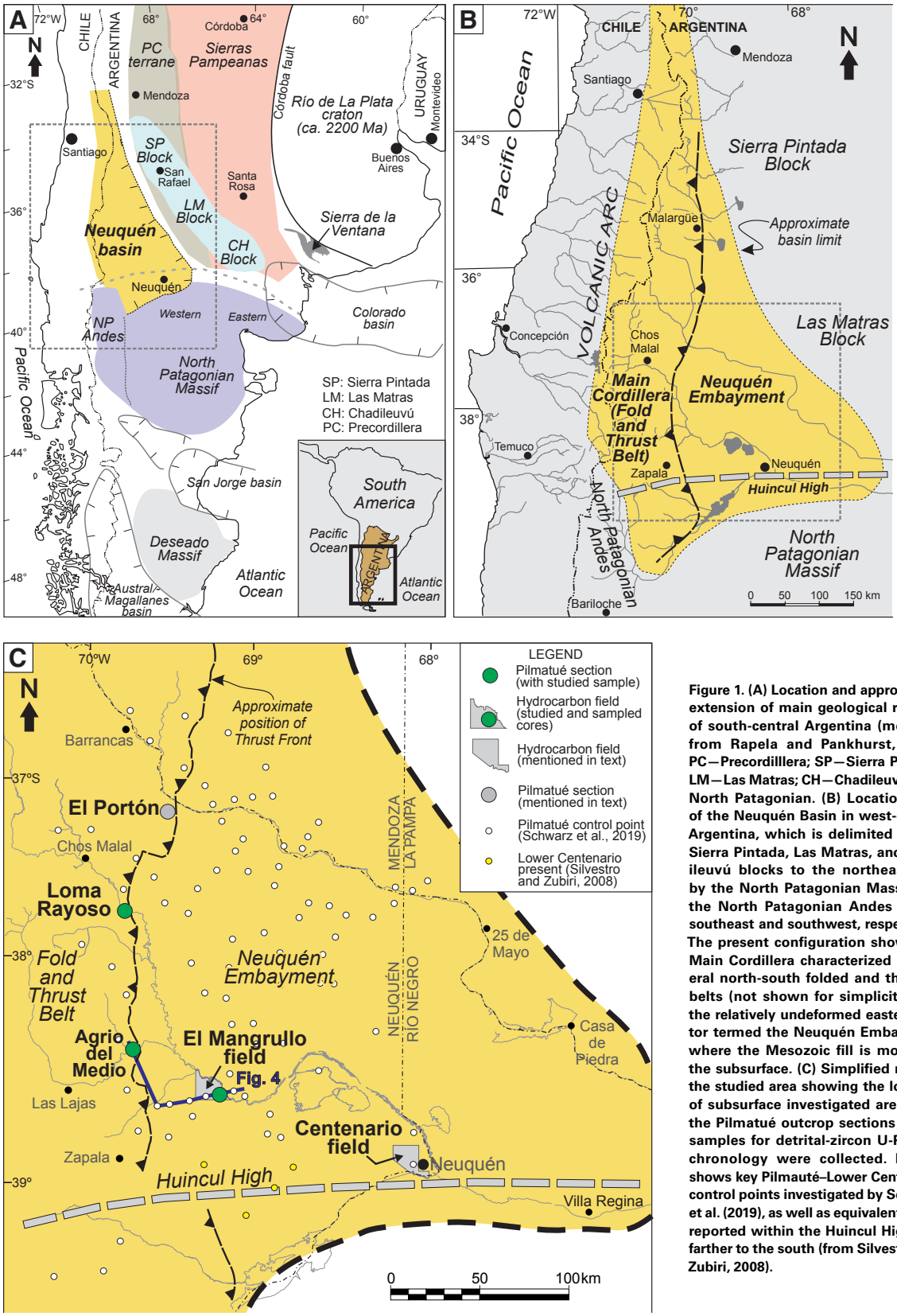

Figure 1. (A) Location and approximate extension of main geological regions of south-central Argentina (modified from Rapela and Pankhurst, 2020). PC—Precordilllera; SP—Sierra Pintada; LM—Las Matras; CH—Chadileuvú; NP—North Patagonian. (B) Location map of the Neuquén Basin in west-central Argentina, which is delimited by the Sierra Pintada, Las Matras, and Chadileuvú blocks to the northeast and by the North Patagonian Massif and the North Patagonian Andes to the southeast and southwest, respectively. The present configuration shows the Main Cordillera characterized by several north-south folded and thrusted belts (not shown for simplicity) and the relatively undeformed eastern sector termed the Neuquén Embayment, where the Mesozoic fill is mostly in the subsurface. (C) Simplified map of the studied area showing the location of subsurface investigated areas and the Pilmatué outcrop sections where samples for detrital-zircon U-Pb geochronology were collected. It also shows key Pilmauté–Lower Centenario control points investigated by Schwarz et al. (2019), as well as equivalent strata reported within the Huincul High and farther to the south (from Silvestro and Zubiri, 2008).

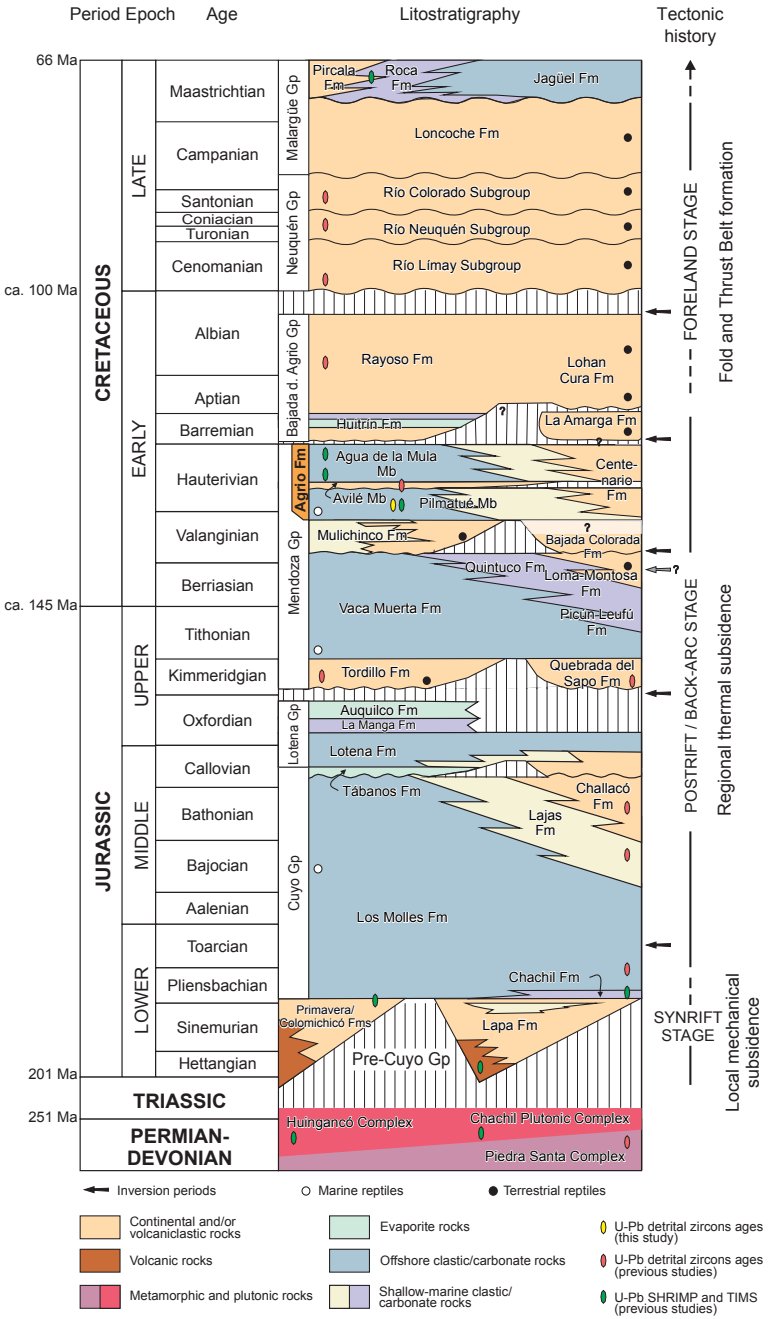

Figure 2. Chronostratigraphy, tectonic history, and biostratigraphic resolution of the Neuquén Basin (modified from Howell et al., 2005). Tectonic history after Vergani et al. (1995) and Franzese et al. (2003). U-Pb isotopic ages and U-Pb detrital-zircon studies mostly compiled from Naipauer and Ramos (2016). The Agrio Formation interval is highlighted in orange.

shallow-marine deposits of the Mulichinco Formation (Schwarz and Howell, 2005). At the top, the Pilmatué Member is abruptly truncated by continental (fluvial and eolian) deposits of the Avilé Member (Fig. 3A), which represents a second-order, lowstand stage of a younger sequence (Legarreta and Uliana, 1991; Veiga et al., 2007, Veiga et al., 2011). The Lower Centenario Member represents the stratigraphic equivalent of the Pilmatué Member in the eastern sector of the Neuquén Embayment (Fig. 3A). In the Centenario field, near Neuquén city (Fig. 1C), this unit is composed of sandstone-dominated fluvial red beds (Fig. 3B), with subordinate mudstones and siltstones (Digregorio, 1972; Uliana et al., 1977). The Pilmatué–Lower Centenario interval varies from 700 m of thickness in the central part of the basin (Lazo et al., 2009; Schwarz et al., 2016), to ~100 m at the marginal sectors located to the NE in the subsurface (Iñigo et al., 2018) and in southernmost outcrops (Luci and Lazo, 2015). The unit is also present (albeit thin) within the tectonically complex Huincul High and the less deformed subsurface sector located to its south (Silvestro and Zubiri, 2008) (Fig. 1C). The tectonic regime for this interval is considered as a sag phase without evidence of inversion or contractional phases (Legarreta and Uliana, 1991; Vergani et al., 1995).

The sedimentology, depositional facies, and paleoenvironments of the Pilmatué Member were recently reported and interpreted from the western sector of the Neuquén Embayment and across several regions of the Main Cordillera (Schwarz et al., 2016; Veiga and Schwarz, 2016; Schwarz et al., 2018a, 2018b; Remírez et al., 2020) (Fig. 3B). In the El Mangrullo area (Fig. 1C), the unit is mostly composed of sandstone-dominated successions interpreted to represent delta-front deposits that commonly grade to sandy channel-fill successions interbedded with

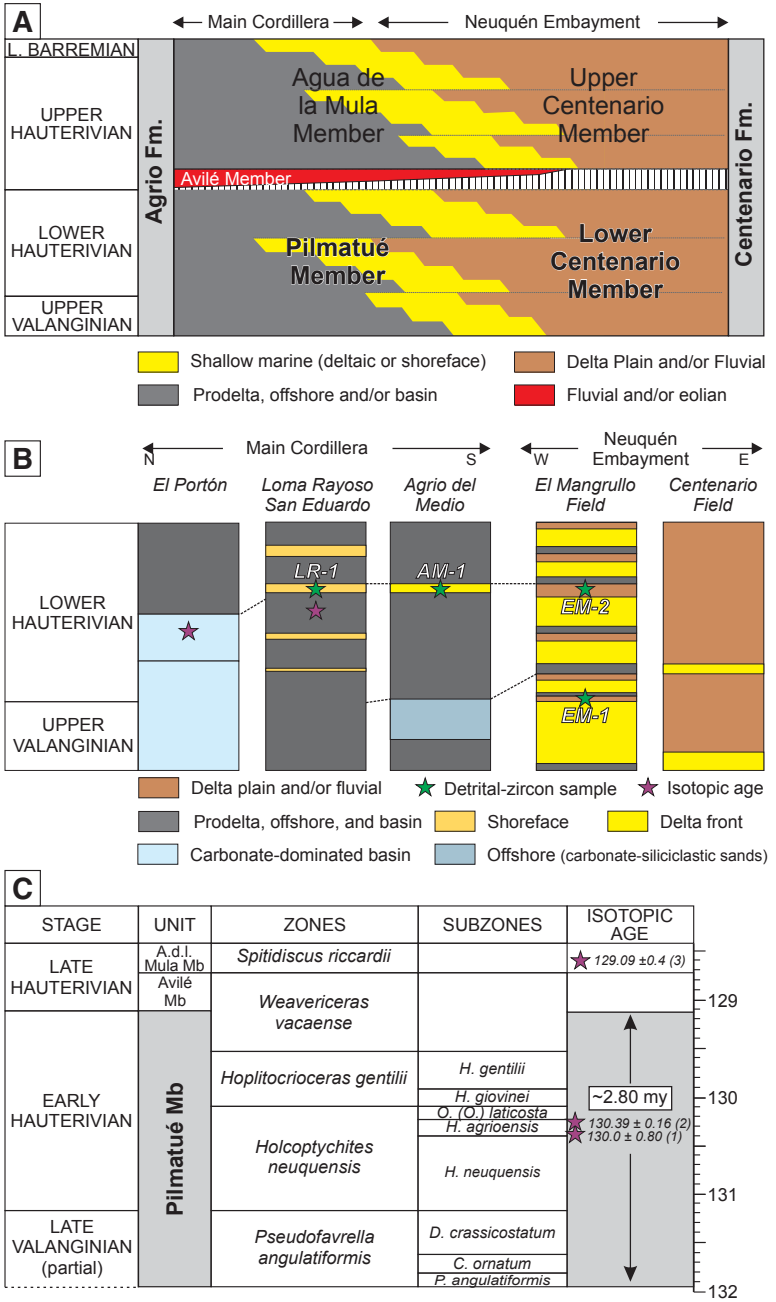

Figure 3. (A) Simplified chronostratigraphic chart of the late Valanginian–early Barremian of the Neuquén Basin, showing the lateral stratigraphic relationships between the Pilmatué Member and the Lower Centenario Member (adapted from Digregorio, 1972; Uliana et al., 1977; Schwarz et al., 2018b). (B) Simplified sedimentary sections of the Pilmatué–Lower Centenario strata across the basin (see Fig. 1C for their location) showing vertical distribution of facies, approximate vertical location of the four samples presented in this contribution, and vertical location of dated tuffs available for the unit. Note that vertical axis is time. Also note the clear proximal-distal trend from east to west and the increment to the north of carbonate contribution in distal marine settings. (C) High-resolution late Valanginian–early Hauterivian biostratigraphic scheme for the Pilmatué Member of the Agrio Formation (compiled from Aguirre-Urreta et al., 2005, 2019). Isotopic ages from the Pilmatué Member as follows: (1) Sensitive high-resolution ion microprobe (SHRIMP) U-Pb age of Schwarz et al. (2016); and (2) thermal ionization mass spectrometry (TIMS) U-Pb age of Aguirre-Urreta et al. (2017). The base of the Agua de la Mula Member is also constrained by a TIMS U-Pb age of Aguirre-Urreta et al. (2015).

mudstones showing subaerial exposure, which are collectively interpreted as delta-plain to fully fluvial settings (Schwarz et al., 2018a) (Fig. 3B). Subordinate prodelta and/or offshore fine-grained deposits delineate major transgressive surfaces within this region. Farther to the east and northeast in the Main Cordillera, the unit becomes dominated by prodelta and/or offshore siliciclastic mudstones with subordinate sandstone intervals that reflect delta-front conditions in the south, but storm-dominated, shoreface settings toward the north (Schwarz et al., 2018b) (Fig. 3B). In the northern Main Cordillera, the Pilmatué Member is largely composed of carbonate-dominated mudstones interpreted to represent more distal, basinal settings within the ramp-type profile of the marine basin (Sagasti, 2005; Schwarz et al., 2018b; Remírez et al., 2020). An overall east-to-west deepening interpreted from the facies (Fig. 4) suggests an eastern sediment source for this area of the basin.

Four ammonite zones can typically be identified in this unit (Aguirre-Urreta et al., 2005, 2011, 2019) providing a high-resolution biostratigraphic framework for the Upper Valanginian–lower Hauterivian strata in the basin (Fig. 3C). This was recently

integrated with absolute ages: tuff layers occurring within the *Holcoptychites neuquensis* Zone delivered an absolute age of 130.0 ± 0.6 Ma (SHRIMP, Schwarz et al., 2016) and 130.39 ± 0.16 Ma (TIMS, Aguirre Urreta et al., 2019) (Fig. 3C). The base of the Agua de la Mula Member is also constrained by a TIMS U-Pb zircon age of 129.09 ± 0.04 Ma (Aguirre-Urreta et al., 2015). The associated *Spitidiscus riccardii* subzone (Fig. 3C) is present across the basin, suggesting a fairly instantaneous transgression, and thus this regionally extensive transgressive surface is used in this contribution as datum (see Fig. 4).

2.2 Pilmatué Member Depositional Stages

The integration of depositional facies, stratal patterns, and key stratigraphic surfaces recognized and interpreted within the Pilmatué Member across the western Neuquén Embayment and the Main Cordillera (Fig. 1C) allowed Schwarz et al. (2019) to subdivide the unit into three main depositional stages, here termed sequences for simplicity (Fig. 4). The facies and paleoenvironmental characterization of these three sequences can be reconstructed across a 65-km-long correlation panel from El Mangrullo Field to the nearest outcrops located in the Agrio del Medio section (Fig. 4). As shown in the correlation panel, the three sequences are dominated by river-dominated or both wave- and river-influenced delta-front deposits in the east, with subordinate delta-plain, prodelta, and offshore deposits. The proportion of delta-plain and delta-front deposits decreases westward, with the coeval increment of prodelta and offshore deposits. Each depositional stage is bounded by a transgressive surface suggesting tens of kilometers of landward displacement of the shoreline (Fig. 4). These three sequences and their bounding surfaces are heavily constrained by ammonite

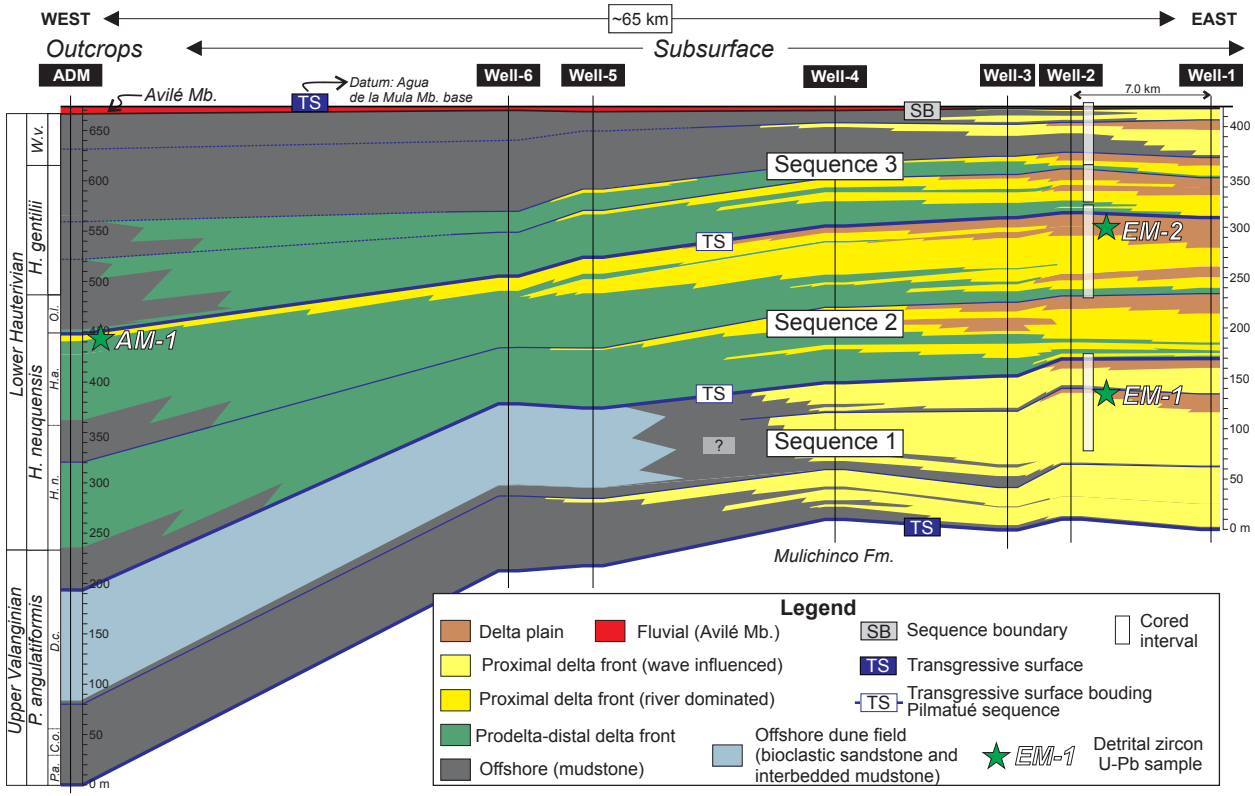

Figure 4. Detailed correlation panel oriented approximately along depositional dip from the El Mangrullo field to the Agrio del Medio anticline (ADM), showing the detailed distributions of facies and the sequence stratigraphic scheme proposed by Schwarz et al. (2019). See Figure 1C for location of correlation panel. Location and stratigraphic position of EM-1, EM-2, and AM-1 samples with detrital-zircon U-Pb geochronology are also indicated. Biostratigraphy of Agrio del Medio section follows Lazo et al. (2009). See Fig. 3C for biozone nomenclature.

biostratigraphy in outcrops (Lazo et al., 2009) and their potential correlation in the subsurface.

In the west (Agrio del Medio Section), Sequence 1 spans most of the *angulatiformis* ammonite zone and includes not only offshore mudstones but also mixed carbonate-siliciclastic sandstones (Fig. 4). These mixed deposits having large-scale cross-bedding and exceptionally preserved crinoids were interpreted to reflect tidally influenced offshore dune fields (Veiga and Schwarz, 2016; Lazo et al., 2020). Sequence 2 in the west spans most of the *neuquensis* and *agrioensis* ammonite subzones and is dominated by offshore, prodelta, and distal-delta front deposits. At its top, a 3-m-thick sandstone package is interpreted as reflecting delta-front deposits (see AM-1 sample description below) and maximum progradation recorded in the system (Fig. 4). Finally, Sequence 3 in the western sector is almost entirely composed of offshore mudstones and spans the *laticosta* subzone to the top of the unit (Fig. 4).

3. DETRITAL-ZIRCON U-Pb GEOCHRONOLOGY

3.1 Sample Collection and Methods

Four sandstones were collected for detrital-zircon analyses from the Pilmatué Member. Sampling was aimed at capturing both vertical and spatial characteristics of the detrital-zircon age patterns within these well-defined sequences. Two of the samples (i.e., EM-1 and EM-2) were taken from subsurface cores in the El Mangrullo hydrocarbon field (Figs. 1C and 4). AM-1 was collected from the Pilmatué section exposed in the Agrio del Medio section, whereas LR-1 was collected form the Loma Rayoso section, located ~50 km to the north (Fig. 1C). Sedimentological, biostratigraphic, and radiometric data (Schwarz et al., 2016, 2018b) place both of these samples at the top of the *agrioensis* subzone (Figs. 3B and 3C). Detailed sample location information is provided in Table 1.

Approximately 6–10 kg of sandstone were collected from each sample site; the subsurface samples were collected from one core box per sample (Fig. 5). Samples were processed using standard mineral separation techniques at the University of Iowa to extract a heavy-mineral separate (e.g., jaw crusher, disk mill, and water table). The separate was sieved using disposable 350 µm screen, and non-zircon was removed by magnetic and density separations. A random aliquot was "negatively" handpicked under alcohol to remove all non-zircon, resulting in a final separate of ~500 grains for each sample that was mounted in a 1-inch epoxy puck. The puck was ground and polished to expose grain interiors, and backscatter electron images were acquired using a Hitachi 3400 scanning electron microprobe (SEM) at the University of Iowa.

Detrital-zircon grains were analyzed for U-Pb isotopes by laser ablation–multicollector–inductively coupled plasma mass spectrometry (LA-MC-ICPMS) at the Arizona LaserChron Center following the methods of Gehrels et al. (2006) and Gehrels (2012). The specific analytical parameters can be found in the Supplemental Material[1]. Zircon grains were ablated using a 20-µm-beam diameter. Three reference materials were used: Sri Lanka (SL) zircon (ca. 563.5 Ma) was the primary standard, and Duluth Gabbro (FC) zircon (ca. 1099 Ma) and R33 (ca. 420 Ma) zircon were secondary standards. Approximately 315 detrital-zircon grains from each sample were analyzed. Data reduction was accomplished using the internal AgeCalc Excel spreadsheet available from the LaserChron Center. Grains that are >400 Ma have been filtered for >20% discordance or >5% reverse discordance and are not included in the discussion of the results. Typical discordance filters for provenance U-Pb detrital-zircon data are 10%–20%; we chose to use 20% in order to include the highest number of dates. When a 10% discordance filter is applied to the data set, <4% of randomly distributed grains are excluded; application of this filter does not affect our interpretation of the data. The $^{206}Pb/^{238}U$ ages are presented for grains younger than 900 Ma, whereas the $^{207}Pb/^{206}Pb$ ages are used for grains older than 900 Ma. Grain size of the dated grains was acquired using photos of the mounts and the chromium offline targeting software. The analytical data are reported in Table S1 (footnote 1).

3.2 Stratigraphic and Paleogeographic Context

Samples EM-1 and EM-2 comprise lower medium- to very fine-grained sandstones typically having planar to low-angle lamination, or cross-stratification, with common soft-sediment deformation structures such as dish structures and convolute bedding (Fig. 5). These sandstone units show erosional bases and fining-upward vertical trends. They are interbedded with mudstone and siltstone showing attributes of subaerial exposure and incipient soil development, such as pedogenic structures, root marks, and slickensides (Fig. 5). In this context, the sampled sandstone units (i.e., EM-1 and EM-2) are interpreted to represent distributary channel deposits (Figs. 4 and 5), within a delta-plain setting situated eastwards of a marine basin shoreline (Schwarz et al., 2018a). The vast majority of the sandstones in these channel fills are upper fine-grained to lower medium-grained, with very rare upper medium-grained or coarser sandstone. Within the pebble grade, mudstone intraclasts are commonly the coarsest fraction (Fig. 5), which suggests that these open channels were capable of transporting upper medium-grained or coarser sand, but this grain-size fraction was not readily available in this part of the depositional system (Schwarz et al., 2018a).

TABLE 1. SAMPLE LOCATION INFORMATION

Sample location	Latitude (°N)	Longitude (°W)	Location description	Key references
EM-1	38°35'11.17"	69°26'56.78"	El Mangrullo Field	Schwarz et al., 2018a
EM-2	38°34'12.36"	69°26'13.20"	El Mangrullo Field	Schwarz et al., 2018a
AM-1	38°22'35.95"	69°58'23.19"	Measured section in Agrio del Medio anticline	Schwarz et al., 2019
LR-1	37°36'25.55"	70° 5'53.24"	Measured section in Loma Rayoso anticline	Schwarz et al., 2018b

[1]Supplemental Material. Table S1: Detrital-zircon data. Please visit https://doi.org/10.1130/GEOS.S.13269392 to access the supplemental material, and contact editing@geosociety.org with any questions.

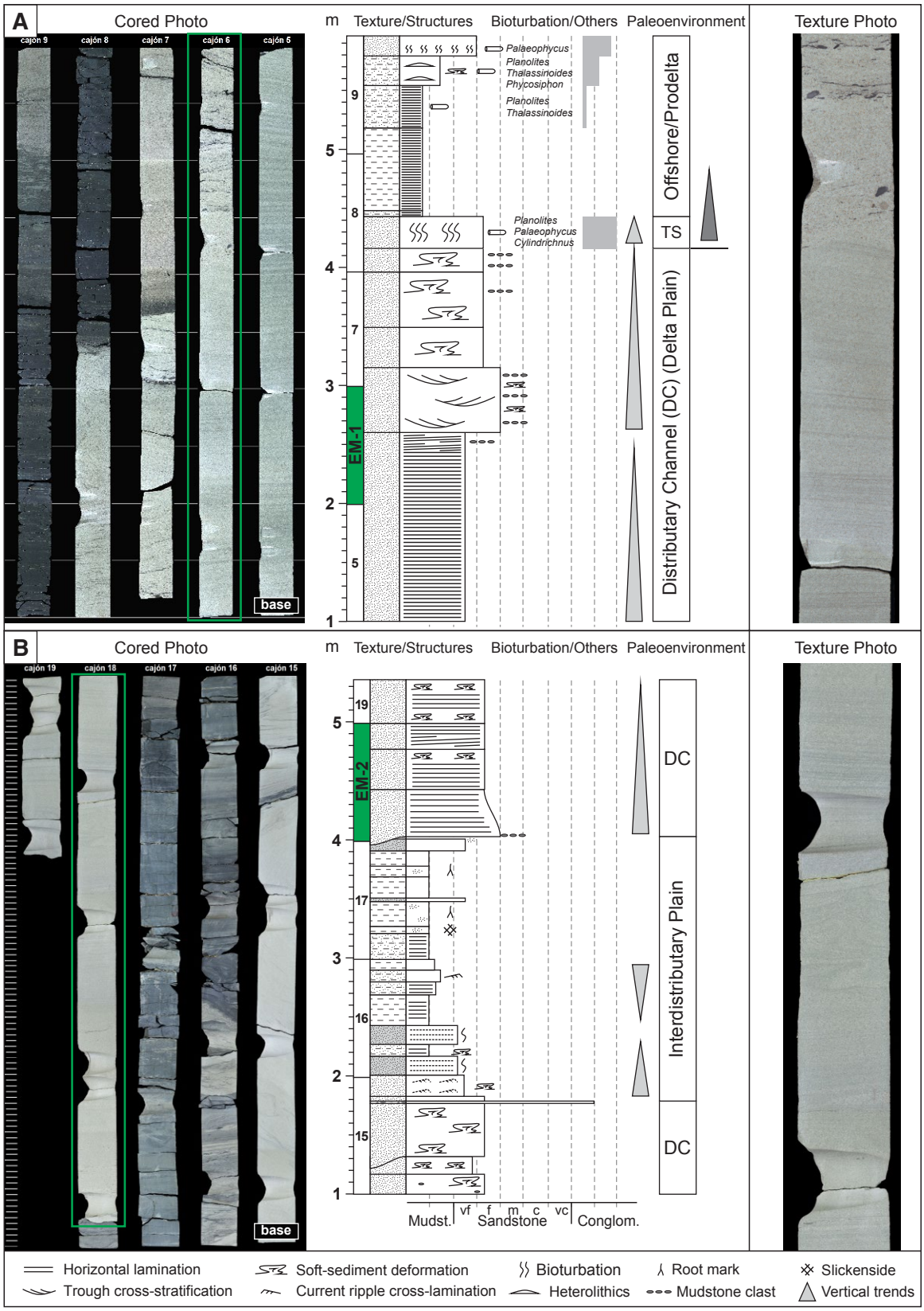

Figure 5. Sedimentologic attributes and facies context of the El Mangrullo subsurface samples (EM-1 and EM-2). (A) EM-1 core photo (marked in green) and simplify sedimentary log with paleoenvironment interpretation. Texture of the sampled core includes very fine-grained sandstone at the base and fine- to lower medium-grained sandstone at the top (right photo). TS—transgressive deposits marking a bounding surface between delta-plain deposits and offshore and/or prodelta deposits. (B) EM-2 core photo (marked in green) and simplify sedimentary log with paleoenvironment interpretation. Texture of sampled core corresponds to fine-grained sandstone (right photo). Both sampled sandstones correspond to a facies association interpreted to represent distributary channels in a delta-plain setting (Schwarz et al., 2018a).

Stratigraphically, EM-1 represents the oldest delta-plain deposits identified in the El Mangrullo field (Fig. 4); these deposits are located near the top of Sequence 1. This interval correlates westwards with mixed (carbonate-siliciclastic) deposits that have large-scale cross-bedding; these deposits are interpreted to reflect tidally influenced, offshore dune fields (Veiga and Schwarz, 2016) (Fig. 6A). EM-2 corresponds to the youngest delta-plain deposits of Sequence 2 (Fig. 4) and reflects the stage of maximum progradation of the shoreline in this region; this stage occurs at the top of this sequence (Fig. 6A). Based on thin-section petrography, the sampled sandstones compositionally range from lithic arkose sandstones to feldspathic litharenites.

AM-1 was collected from lower fine-grained sandstone showing current ripple cross-lamination and planar lamination with parting lineation, very low bioturbation, and abundant soft-sediment deformation (Figs. 7A and 7B). This 3 m sandstone package grades from thinly interbedded mudstone and sandstone heterolithics having wave and combined-flow ripples and low bioturbation represented by small *Skolithos* burrows. Facies and vertical trends suggest that this coarsening-upward package most probably represents accumulation as a fluvio-dominated mouth bar in a delta-front setting (Schwarz et al., 2019). This sand-rich interval is unique within the overall mudstone-dominated succession exposed in the Agrio del Medio anticline (Lazo et al., 2009) and is therefore correlated to the maximum progradation identified within the El Mangrullo field (top of Sequence 2, Fig. 4).

The Loma Rayoso section has more sandstone-dominated intervals than Agrio del Medio Section (Fig. 3B), but these intervals commonly show a high degree of bioturbation, as well as wave- and storm-related structures. LR-1 comprises a lower fine-grained sandstone, within one of these highly bioturbated intervals (*Skolithos* ichnofacies), with uncommon preservation of hummocky cross-stratification and wave-ripple lamination (Figs. 7C and 7D). These bioturbated sandstone packages represent terrigenous sediments accumulated in a storm- and wave-dominated lower shoreface within a shoreface-basin system developed farther to the north of the other sample sites (Schwarz et al., 2018b). Because both AM-1 and LR-1 occur at the top of the *agrioensis* subzone, they are interpreted to represent the expression of coeval shallow-marine sedimentation during the maximum progradation associated with Sequence 2 (Fig. 6B). In the northern vicinity of LR-1, terrigenous sands are commonly mixed with ooids and bioclasts in the upper-shoreface setting, suggesting minimal direct input from co-located terrestrial systems and, instead, the development of an along-shore sediment dispersal system distributing siliciclastic sands from south to north (Schwarz et al., 2018b) (Fig. 6B).

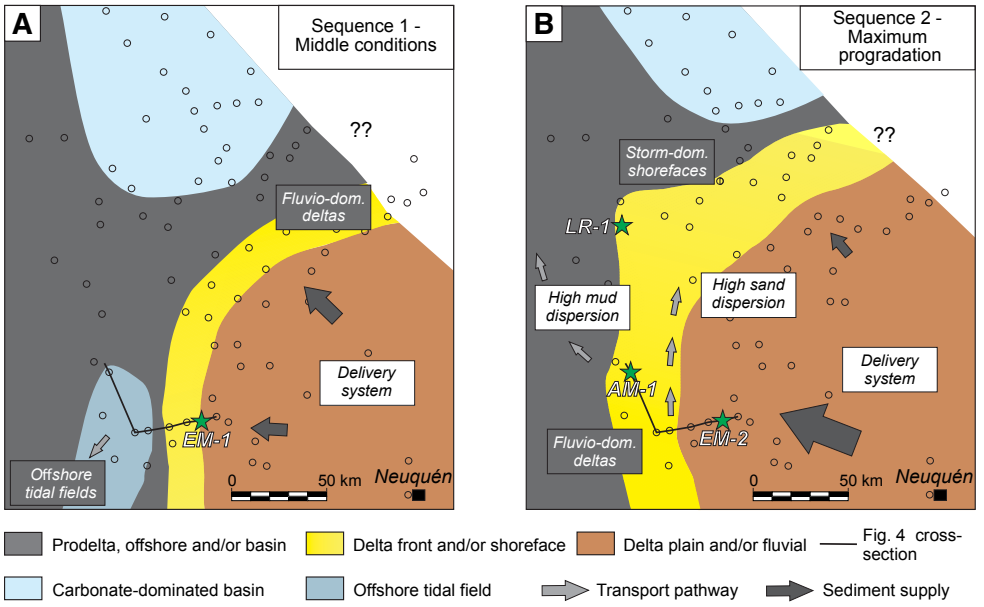

Figure 6. Regional paleogeographic reconstruction for the Pilmatué Member based on ~20 outcrop locations and ~150 wells (after Schwarz et al., 2019). (A) Reconstructed paleogeography for EM-1 sandstone times, which correspond to middle conditions of Sequence 1 (*D. crassicostatum* subzone). (B) Reconstructed paleogeography that involves EM-2, AM-1, and LR-2 sandstone period, which corresponds to maximum progradation associated to Sequence 2 (*H. agrioensis* subzone). Note that though the locus of deltaic development changes through time (fluvio-dominated deltas), there is a clear proximal-distal depositional trend from southeast to northeast.

4. DETRITAL-ZIRCON U-Pb GEOCHRONOLOGY RESULTS

The detrital-zircon age distributions obtained from the four samples are generally similar ranging from ca. 130–3300 Ma with differences in abundances in only some age groups (Fig. 8A). Four Phanerozoic age populations are recognized in all of the samples: Early Jurassic (ca. 175–190 Ma), Early Triassic to Early Permian (ca. 245–300 Ma), Ordovician (ca. 450–485 Ma), and Cambrian (ca. 510–540 Ma) (Fig. 8A). These age populations typically represent 8%–20% of the dated detrital-zircon grains in each sample, but the Triassic–Permian population reaches up to 27% in the outcrop examples (Fig. 8B). Late Jurassic to Early Cretaceous zircon grains (<178 Ma) are very rare and represent 1%–3%, and the same is true for zircon grains with Silurian to Carboniferous ages, which correspond to 4%–6% of each sample (Fig. 8).

The detrital-zircon ages of the four samples also show a consistent pattern in Proterozoic grain

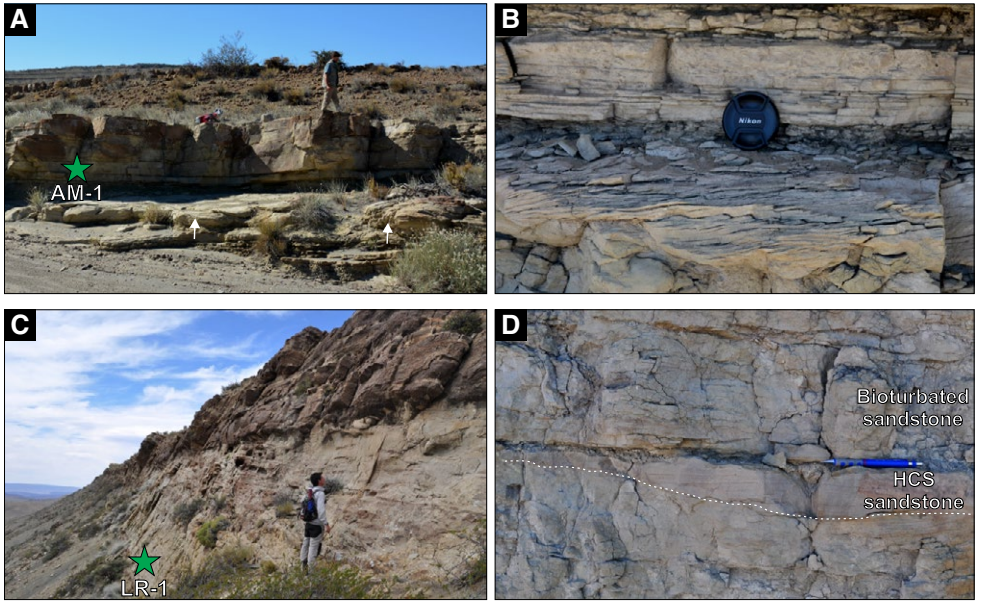

Figure 7. Sedimentologic attributes and facies context of outcrop AM-1 and LR-1 sandstones. (A) Sandstone package of AM-1 sample, characterized by current ripple cross-lamination, abundant soft-sediment deformation (white arrows), and very low bioturbation, interbedded within a thick succession of prodelta and offshore mudstones. Person for scale. (B) Fine-grained sandstone with current ripple cross-lamination overlain by sandstone bed with horizontal lamination, collectively interpreted to represent unidirectional-dominated currents in a fluvio-dominated delta-front setting. Lens cap for scale is 5 cm wide. (C) Sandstone package of LR-1 sample, showing a gradual, upward coarsening trend from offshore mudstones. Person for scale. (D) Detailed facies context of LR-1 sample, showing intensively bioturbated and hummocky cross-stratified (HCS)sandstones, interpreted to represent a storm-dominated, lower-shoreface setting (Schwarz et al., 2018b).

populations (Fig. 8A). Late Neoproterozoic zircon grains of Ediacaran age (541–635 Ma) typically represent ~14% in the subsurface samples (EM-1 and EM-2) and slightly decrease in the outcrop samples to 10%. The majority of these grains range ca. 580–635 Ma (Fig. 8A). Combined with Early to Middle Neoproterozoic zircon grains (636–1000 Ma), these Neoproterozoic ages represent 20%–26% of the entire population in each sample (Fig. 8B). All samples also show a significant population of Late Mesoproterozoic zircon grains (1000–1200 Ma); these grains represent 9%–14% of the total and primarily range from 1000 to 1100 Ma (Fig. 8). Older zircon grains (>1200 Ma) are uncommon in all samples and represent only 4%–8%.

Dated zircon grains are mostly in the very fine size range; mean long crystal axis lengths vary from 0.11 to 0.062 mm (Fig. 9). When plotted by age groups, the mean size of each age group typically falls within the interquartile range of all the zircon grains for that sample, and there is no clear trend between specific age groups and grain size as estimated by the long axis length. Given the uniformity of the size data (Fig. 9), we do not expect significant biasing of the age distributions as was recently highlighted by a detrital-zircon study in a modern river (e.g., Ibañez-Mejia et al., 2018). That said, the distal samples (AM-1 and LR-1) have mean grain sizes in the lower very fine range (average 0.062 and 0.070 mm, respectively), whereas the proximal samples (EM-1 and EM-2) are in the upper very fine range (0.083 and 0.110 mm, respectively; Fig. 9), reflecting typical downstream fining in the sedimentary system but without age group biasing.

5. PROVENANCE INTERPRETATION

The present-day configuration of the Neuquén Basin (Figs. 1B and 1C) illustrates a heavily deformed western sector (Main Cordillera) characterized by thick Jurassic and Cretaceous strata forming a fold and thrust belt (Ramos, 1999) and a relatively less deformed Neuquén Embayment to the east in which the same stratigraphy is present in the subsurface. The interpretation of the most probable sources for the different detrital-zircon populations identified in the Pilmatué Member samples requires not only an understanding of the distribution of rocks around and within the Neuquén Basin (Fig. 10, Table 2) but also comprehensive knowledge about the paleogeographic reconstructions and potential sediment-dispersal patterns based on the sedimentology (Fig. 6). The detailed sedimentologic and stratigraphic studies on these units clearly show that EM-1 and EM-2 represent delta-plain to fluvial (proximal) settings (Schwarz et al., 2018a) that should retain a direct connection to their sediment source areas, whereas AM-1 and LR-1 reflect accumulation in shallow-marine (i.e., more distal) conditions where mixing from other sources is possible. This reconstruction suggests a long-lived (~3 m.y.) delivery system of siliciclastics coming from the southeastern margin of the basin; this system was able to transport solely medium-grained and finer sediment across the entire extent of the Neuquén Basin. Sediment flux from the western margin of the basin was unlikely given the offshore marine clastic and carbonate depositional conditions there (Sagasti, 2005; Remírez et al., 2020).

Considering this reconstruction and the main position of the delivery system in the southeast sector of the basin, it is possible to restrict the potential sediment sources for the Pilmatué sands. In this sense, the geological terranes that are considered and discussed here are: the North

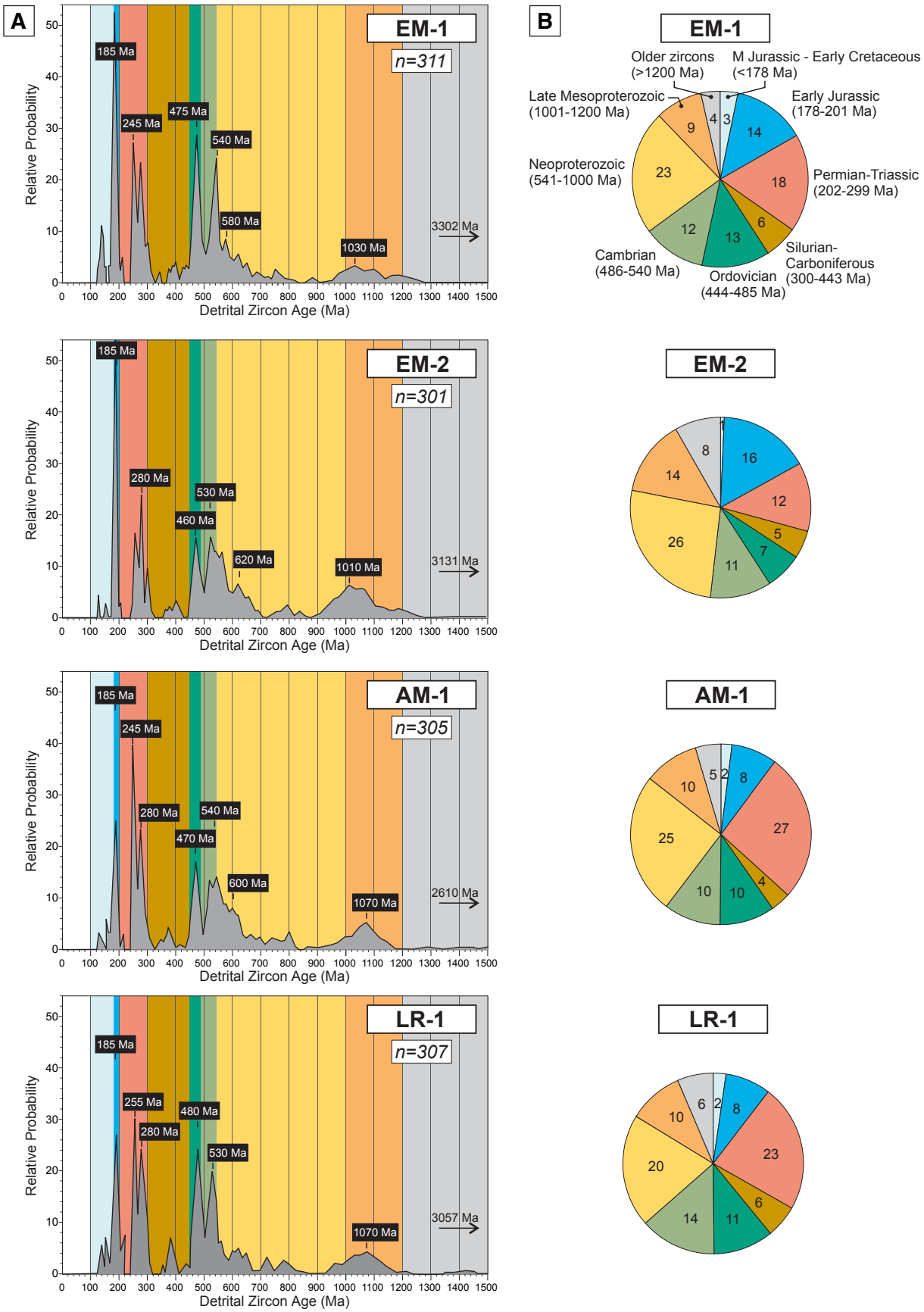

Figure 8. (A) Normalized relative age probability diagrams of detrital-zircon data (made with Isoplot). Colored rectangles illustrate age ranges of potential source terranes, and colors coordinate with rock groups shown in Figures 9 and 10. n—number of grains. (B) Pie charts showing the percentages of zircon grains that plot within the nine age groups defined in this contribution. Age range details in EM-1 pie chart.

Patagonian Andes, the North Patagonian Massif (NPM), the Chadileuvú Block and the southern sector of the Las Matras Block, and the Sierra de la Ventana Belt and Río de La Plata Craton farther to the east (Figs. 1A and 10). For the purpose of this study, the North Patagonian Massif is further divided into a western sector and an eastern sector. The western sector is dominated by Permian and Triassic rocks, whereas the eastern sector has more variability from Cambrian to Lower Jurassic rocks (Fig. 10). We also include a simplified geological map and detrital-zircon U-Pb ages from the Saldania Belt located in southern South Africa; during Hauterivian time, this Belt was located southeast of the North Patagonian Massif (Macdonald et al., 2003; Pángaro and Ramos, 2012; Will and Frimmel, 2018) (inset in Fig. 10).

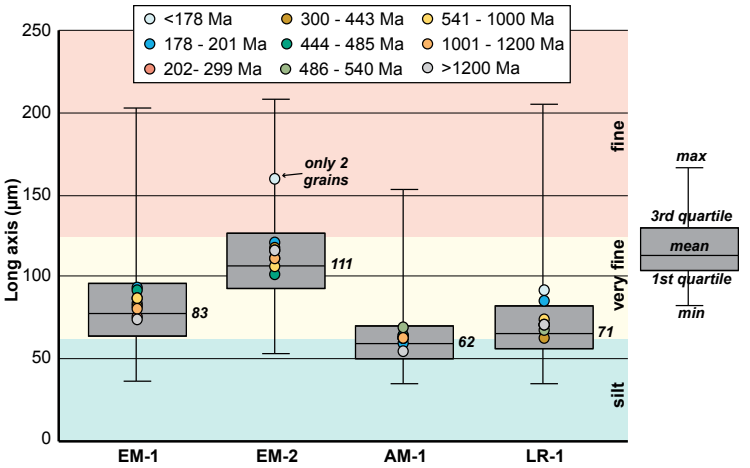

Figure 9. Plots of mean and ranges of detrital-zircon grain sizes. The colored dots are the mean for each age group discussed in the text. The gray boxes represent the mean (horizontal black line), first and third quartiles (gray box), and total range (error bars) of grain sizes for all the zircon grains in each sample.

5.1 Early Jurassic (Ca. 175–190 Ma) Sources

5.1.1 Potential Sources

This age population is present in all of the samples, decreasing from 16% to 8% from the proximal (EM-1 and EM-2) to distal (LR-1 and AM-1) settings; the main peak in the distribution is ca. 185 Ma (Figs. 8 and 9). These ages correlate well with the V1 group of the large Chon Aike magmatic province of the eastern sector of the North Patagonian Massif (Pankhurst and Rapela, 1995; Pankhurst et al., 2000). The rhyolite rocks of this group crop out extensively in northeastern Patagonia (Fig. 10) and are known as the Marifil Formation and/or Complex. Original Rb-Sr ages and more recent U-Pb ages suggest a crystallization age ranging from ca. 178–190 Ma (Pankhurst et al., 2000; Strazzere et al., 2017). Pavón Pivetta et al. (2019, and references therein) compiled all the available geochronological data from northeast Patagonia and corroborated the crystallization age for V1 but identified a possible initial volcanic stage that went back to 192.6 ± 2.5 Ma.

There are similar Early Jurassic ages found in the North Patagonian Andes from granitoids of the so-called Subcordilleran belt (181–185 Ma, Fig. 10) (Rapela et al., 2005). According to Rapela et al. (2005), geochemical and isotopic data suggest that these plutonic rocks are associated with an Early Jurassic subduction-related magmatic arc along the proto-Pacific margin of Gondwana, approximately synchronous with the V1 phase of the Chon Aike magmatism. In addition, there are also volcanic rocks of the synrift stage of the Neuquén Basin, known as the Precuyano Cycle, with Early Jurassic ages (Fig. 10). In the subsurface of the southern sector of the basin, a dacite lava was dated as 199.0 Ma, whereas exposed acidic lavas from the northwestern sector (northwest of Chos Malal, Fig. 10) were dated as 181–187 Ma (Zappettini et al., 2019) (Table 2). Significantly, there is no evidence for Early Jurassic magmatic rocks in central Argentina (Chadileuvú Block or farther to the north in Las Matras and San Rafael Blocks) or on the eastern margin of Argentina (Río de La Plata Craton, Fig. 10). In South Africa, however, the Karoo volcanic province presently exposed extensively eastwards of the Cape Fold Belt comprises Early Jurassic volcanics with crystallization ages of 179–184 Ma (Table 2). These volcanic rocks are mainly composed of basaltic lavas, although subordinate rhyolites with similar ages are also described (Riley et al., 2004).

5.1.2 Interpretation

Considering all of the available data, we interpret that the volcanic rocks of the Marifil Complex located in the eastern sector of the NPM were the major supplier of the Early Jurassic zircon grains that were eventually incorporated in the Pilmatué sandstones. The paleogeographic reconstruction of the Pilmatué depositional systems would make a western source unlikely for this zircon population (Fig. 6), either from the North Patagonian Andes (Subcordilleran belt) or the northwestern Neuquén Basin region. Furthermore, the decay of the proportion of this population from the southern proximal to northern distal samples (Fig. 8B) also suggests that a southeastern source is more likely. The synrift volcanics within the Neuquén Basin are typically covered by hundreds of meters of postrift strata even in the southeast and northeast marginal areas of the basin (e.g., Iñigo et al., 2018), and therefore they are not likely candidates for providing Early Jurassic zircon grains to the Valanginian–Hauterivian Pilmatué strata. Additionally, the oldest Upper Triassic synrift rocks are not represented in

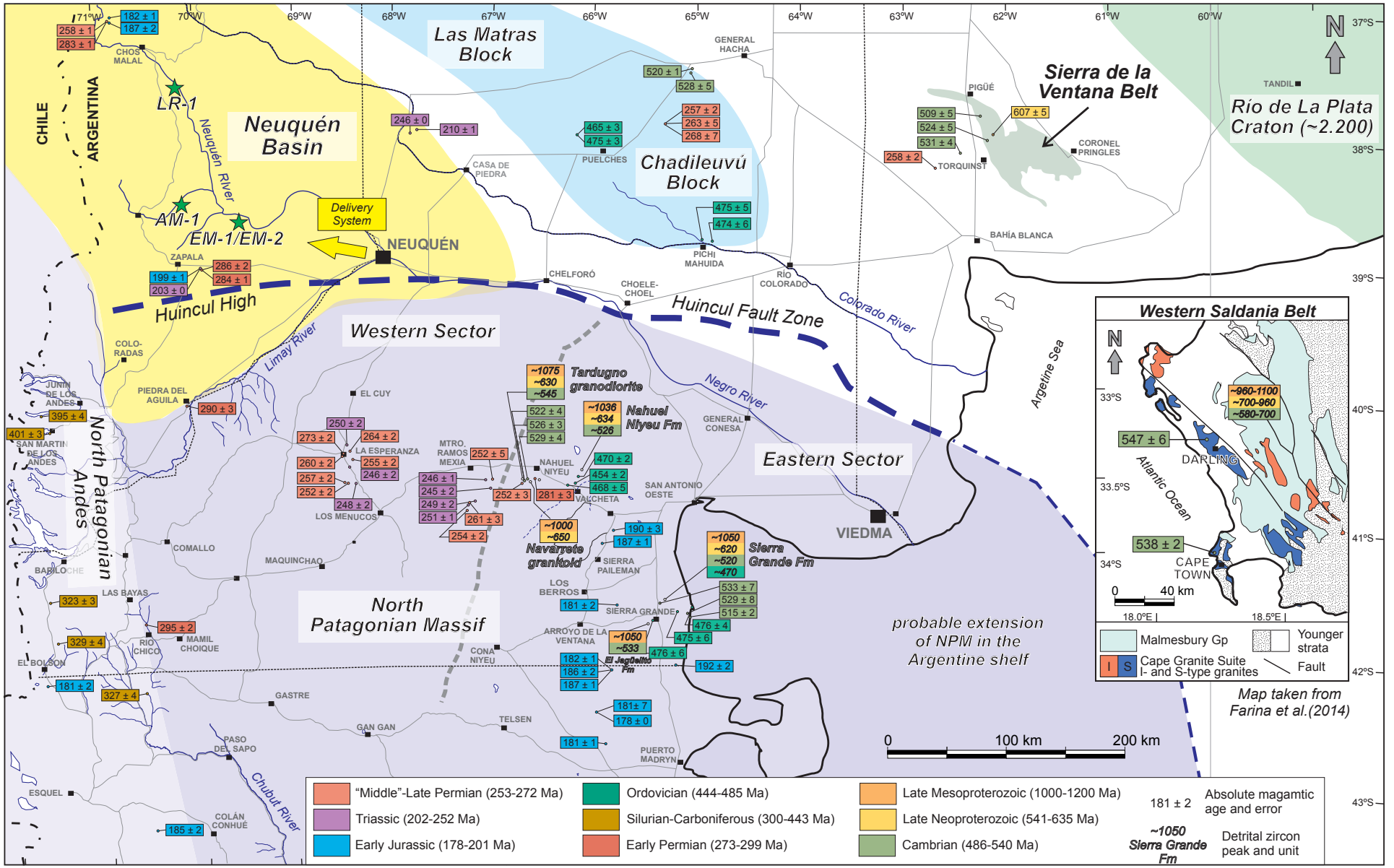

Figure 10. Simplified map of the basement geology and U-Pb zircon ages of central Argentina between 37° and 43° South. Representative ages are indicated in the map, mentioned in the text, and listed in Table 2. Detrital-zircon peaks of selected Paleozoic metasedimentary and sedimentary units, as well as from Paleozoic plutonic rocks, are also indicated. Their references are cited in the text. Inset: simplified map of southernmost South Africa, showing the Saldania Belt (map after Farina et al., 2014), and selected isotopic and detrital-zircon data.

TABLE 2. REPRESENTATIVE ISOTOPIC AGES AVAILABLE FOR PROTEROZOIC TO EARLY CRETACEOUS ROCKS OF CENTRAL ARGENTINA, SEPARATED BY GEOLOGICAL PROVINCES AS SHOWN IN FIGURE 10

Geological province, period, and reference	Age	Error	Method	Rock	Unit
Neuquén Basin					
Lower Jurassic (178–201 Ma)					
Zapettini et al., 2019	181.2	2.4	U-Pb SHRIMP	Tuff layer	Colomichicó (Upper Section)
Zapettini et al., 2019	182.5	0.9	U-Pb SHRIMP	Rhyolite Porfido	Colomichicó (Upper Section)
Zapettini et al., 2019	185.7	2.3	U-Pb SHRIMP	Dacite	Colomichicó (Lower Section)
Zapettini et al., 2019	187.9	1.8	U-Pb SHRIMP	Rhyolite	Colomichicó (Lower Section)
Schiuma and Llambías, 2008	199.0	1.5	U-Pb SHRIMP	Dacite	Precuyano Cycle
Triassic–Permian (202–299 Ma)					
Schiuma and Llambías, 2008	203.7	0.26	U-Pb SHRIMP	Andesite lava	Precuyano Cycle
Barrionuevo et al., 2013	210.9	1.0	U-Pb SHRIMP	Andesitic lava	Precuyano Cycle
Barrionuevo et al., 2013	245.6	0.4	U-Pb SHRIMP	Rhyolitic ignimbrite	Choiyoi Complex
Sato et al., 2008	258.5	1.0	Conventional U-Pb	Monzogranite	Huingancó Complex
Sato et al., 2008	283.4	1.0	Conventional U-Pb	Granodiorite	Huingancó Complex
Schiuma and Llambías, 2008	284.0	1.3	U-Pb SHRIMP	Andesite dike	Choiyoi Complex
Schiuma and Llambías, 2008	286.5	2.3	U-Pb SHRIMP	Granodiorite	Choiyoi Complex
North Patagonian Andes					
Lower Jurassic (178–201 Ma)					
Rapela et al., 2005	181.0	2.0	U-Pb SHRIMP	Granitoid	N/A
Rapela et al., 2005	185.0	2.0	U-Pb SHRIMP	Granitoid	N/A
Silurian–Carboniferous (300–443 Ma)					
Pankhurst et al., 2006	323.0	3.0	U-Pb SHRIMP	N/A	N/A
Pankhurst et al., 2006	329.0	4.0	U-Pb SHRIMP	Granodiorite	Cordon del Serrucho granitoids
Pankhurst et al., 2006	330.0	4.0	U-Pb SHRIMP	Granodiorite	Cordon del Serrucho granitoids
Pankhurst et al., 2006	395.0	4	U-Pb SHRIMP	Granite	Lago Lolog
Pankhurst et al., 2006	401.0	3.0	U-Pb SHRIMP	Tonalite	San Martín Tonalite
North Patagonian Massif—Western Sector					
Triassic–Permian (202–299 Ma)					
Pankhurst et al., 2006	246.0	2.0	U-Pb SHRIMP	Rhyolite	La Esperanza Complex
Tohver et al., 2008	245.0	2.0	N/A	Granitoid	Ramos Mejía Igneous Complex
Tohver et al., 2008	246.0	1.0	N/A	Granitoid	Yaminue Complex
Luppo et al., 2018	248.0	2.0	U-Pb SHRIMP	Dacitic ignimbrite	Los Menucos Complex
Pankhurst et al., 2014	249.0	2.0	U-Pb SHRIMP	Granitoid	Yaminue Complex
Pankhurst et al., 2006	250.0	2.0	U-Pb SHRIMP	Granite	Calvo Granite
Pankhurst et al., 2014	251.0	1.0	U-Pb SHRIMP	Granitoid	Yaminue Complex
Luppo et al., 2018	252.0	2.0	U-Pb SHRIMP	Andesite	Los Menucos Complex
Martínez Dopico et al., 2016	252.0	5.0	U-Pb SHRIMP	Granite	Cabeza de Vaca Leucogranite
Martínez Dopico et al., 2017	254.0	2.0	U-Pb SHRIMP	Granitoid	Yaminue Complex
Martínez Dopico et al., 2017	255.0	2.0	U-Pb SHRIMP	Granodiorite	Prieto Granodiorite
Luppo et al., 2018	257.0	2.0	U-Pb SHRIMP	Rhyolitic ignimbrite	Los Menucos Complex
Martínez Dopico et al., 2017	260.0	2.0	U-Pb SHRIMP	Granite	Donosa Granite
Chernicoff et al., 2012	261.0	3.0	U-Pb SHRIMP	Granitoid	N/A
Pankhurst et al., 2006	264.0	2.0	U-Pb SHRIMP	Rhyolite dome	La Esperanza Complex
Pankhurst et al., 2006	273.0	2.0	U-Pb SHRIMP	Granodiorite	Prieto Granodiorite
Pankhurst et al., 2006	290.0	3.0	U-Pb SHRIMP	Granite	Piedra del Aguila granite
Pankhurst et al., 2006	295.0	2.0	U-Pb SHRIMP	Granite	Tunnel Tonalite

(*continued*)

TABLE 2. REPRESENTATIVE ISOTOPIC AGES AVAILABLE FOR PROTEROZOIC TO EARLY CRETACEOUS ROCKS OF CENTRAL ARGENTINA, SEPARATED BY GEOLOGICAL PROVINCES AS SHOWN IN FIGURE 10 (*continued*)

Geological province, period, and reference	Age	Error	Method	Rock	Unit
North Patagonian Massif–Eastern Sector					
Lower Jurassic (178–201 Ma)					
Alric et al., 1996	178.7	0.4	Ar-Ar	Rhyolite	Marifil Complex
Alric et al., 1996	181.7	1.2	Ar-Ar	Rhyolite	Marifil Complex
Rapela and Pankhurst,1993	181.4	7.1	Rb-Sr	Rhyolite	Marifil Complex
Pankhurst and Rapela, 1995	181.2	2.2	Rb-Sr	Rhyolite	Marifil Complex
Rapela and Pankhurst,1993	182.6	1.5	Rb-Sr	Rhyolite	Marifil Complex
Alric et al., 1996	186.2	3.0	Ar-Ar	Rhyolite	Marifil Complex
Alric et al., 1996	187.4	1.2	Ar-Ar	Rhyolite	Marifil Complex
Pankhurst and Rapela, 1995	187.7	1.3	Rb-Sr	Rhyolite	Marifil Complex
Strazzere et al., 2017	190.6	3.2	U-Pb	Rhyolite	Marifil Complex
Pavón Pivetta et al., 2019	192.6	2.5	U-Pb	Rhyolite	Puesto Iris
Triassic-Permian (202–299 Ma)					
Pankhurst et al., 2014	252.0	3.0	U-Pb SHRIMP	Granitoids	Madsen Tonalite
Pankhurst et al., 2006	281.0	3.0	U-Pb SHRIMP	Granodiorite	Navarrete Granodiorite
Ordovician (444–485)					
Tohver et al., 2008	454.0	2.0	Ar-Ar (Ms)	Granite	Valcheta Granite
Tohver et al., 2008	468.0	5.0	Ar-Ar (Ms)	Granite	Valcheta Granite
Gozálvez, 2009	470.5	1.8	Ar-Ar (Ms)	Leucogranite	Valcheta Granite
Pankhurst et al., 2006	475.0	6.0	U-Pb SHRIMP	Granite	Arroyo Salado Granite
Pankhurst et al., 2006	476.0	6.0	U-Pb SHRIMP	Granite	Sierra Grande Granite
Pankhurst et al., 2006	476.0	4.0	U-Pb SHRIMP	Granite	Punta Bahía Granite
Cambrian (486–540 Ma)					
Pankhurst et al., 2014	522.0	4.0	U-Pb SHRIMP	Granodiorite	Tardugno Granodiorite
Pankhurst et al., 2014	526.0	3.0	U-Pb SHRIMP	Granodiorite	Tardugno Granodiorite
Rapalini et al., 2013	528.5	3.5	U-Pb SHRIMP	Granodiorite	Tardugno Granodiorite
Gonzalez et al., 2018	515.0	2.2	U-Pb SHRIMP	K bentonite	El Jagüelito Formation
Gonzalez et al., 2018	529.4	8.4	U-Pb ICP-MS	Rhyolitic ignimbrite	El Jagüelito Formation
Gonzalez et al., 2018	532.9	7.3	U-Pb SHRIMP	K bentonite	El Jagüelito Formation
Chadileuvu Block					
Triassic–Permian (202–299 Ma)					
Domeier et al., 2011	257.0	2.8	U-Pb SHRIMP	Trachyandesite	Sierra Chica Complex
Domeier et al., 2011	263.0	5.7	U-Pb SHRIMP	Rhyolite ignimbrite	Sierra Chica Complex
Domeier et al., 2011	268.1	7.7	U-Pb SHRIMP	Rhyolite ignimbrite	Sierra Chica Complex
Ordovician (444–485)					
Pankhurst et al., 2006	474.0	6.0	U-Pb SHRIMP	Granite	Rio Colorado Granite
Pankhurst et al., 2006	475.0	5.0	U-Pb SHRIMP	Granite	Curaco Granite
Chernicoff et al., 2010	465.0	3.0	U-Pb SHRIMP	Metagabbro	Paso del Bote granitoids
Chernicoff et al., 2010	475.3	2.3	U-Pb SHRIMP	Metadiorite	Paso del Bote granitoids
Cambrian (486–540 Ma)					
Chernicoff et al., 2012	520.0	1.4	U-Pb SHRIMP	Metadiorite	El Carancho Igneous Complex
Chernicoff et al., 2012	528.0	5.0	U-Pb SHRIMP	Metapyroxenite	El Carancho Igneous Complex

(*continued*)

TABLE 2. REPRESENTATIVE ISOTOPIC AGES AVAILABLE FOR PROTEROZOIC TO EARLY CRETACEOUS ROCKS OF CENTRAL ARGENTINA, SEPARATED BY GEOLOGICAL PROVINCES AS SHOWN IN FIGURE 10 (*continued*)

Geological province, period, and reference	Age	Error	Method	Rock	Unit
Sierra de la Ventana Belt					
Triassic–Permian (202–299 Ma)					
Pankhurst et al., 2006	258.0	2.0	U-Pb SHRIMP	Syenite	López Lecube syenite
Cambrian (486–540 Ma)					
Rapela et al., 2003	509.0	5.3	U-Pb SHRIMP	Rhyolite	La Ermita Rhyolite
Rapela et al., 2003	524.3	5.3	U-Pb SHRIMP	Granite	San Mario Granite
Rapela et al., 2003	531.1	3.1	U-Pb SHRIMP	Granite	Cerro Colorado Granite
Neoproterozoic (541–1000 Ma)					
Rapela et al., 2003	607.0	5.2	U-Pb SHRIMP	Granite	Cerro del Corral Granite
Saldania Belt					
Lower Jurassic (178–201 Ma)					
Riley et al., 2004 in Rapela et al. 2005	180.0	2.0	U-Pb SHRIMP	Rhyolite	Karoo volcanic province
Riley et al., 2004 in Rapela et al. 2005	182.0	3.0	U-Pb SHRIMP	Rhyolite	Karoo volcanic province
Cambrian (486–540 Ma)					
Chemale et al., 2011	524.0	5.0	U-Pb single crystal	A-type granite	N/A
Chemale et al., 2011	510.0	4.0	U-Pb single crystal	A-type granite	N/A
Da Silva et al., 2000	536.0	5.0	U-Pb SHRIMP	I-type granite	Robertson Pluton (Type I)
Farina et al., 2014	537.8	1.6	U-Pb ICP-MS	S-type granite	Peninsula Pluton
Da Silva et al., 2000	547.0	6.0	U-Pb SHRIMP	S-type granite	Darling Pluton

Note: Italicized terms represent the group ages discussed in the text; not all are present in the different regions. Abbreviations: ICP—inductively coupled plasma; MS—mass spectrometry; SHRIMP—sensitive high-resolution ion microprobe; ms—muscovite.

the Pilmatué zircon grains (discussed below). The Pilmatué delivery system could have incorporated some Karoo basaltic volcanics that were attached to Patagonia in the Hauterivian, but only the less common rhyolites would have provided a significant number of zircon grains to the Pilmatué system based on average zircon fertilities of igneous rocks. In any case, the true extent of the northeastern Patagonia rhyolitic plateau in southwestern Gondwana is not well defined and could have easily extended to the east under the present Argentine continental shelf (Lovecchio et al., 2019) (Fig. 10).

5.2 Early Triassic to Early Permian (Ca. 245–300 Ma) Sources

5.2.1 Potential Sources

Pilmatué detrital-zircon grains have a predominance of Early Triassic to Early Permian ages with peaks ca. 245–255 and 280 Ma (Fig. 8A). The proportion of this age population slightly decreases with time in the proximal zone (from EM-1 to EM-2) but increases spatially from the proximal to the distal localities (Fig. 8B). Significantly, Middle and Late Triassic zircon grains (201–240 Ma) are very rare in the four samples despite the fact that synrift volcanics of Late Triassic age (ca. 203–210 Ma) are commonly reported from the Main Cordillera and Embayment of the Neuquén Basin (Fig. 10).

Early Triassic to Early Permian plutonic and volcanic rocks are widespread in central western Argentina and are known as the Choiyoi magmatic province. This belt is interpreted as the most conspicuous feature along the Late Paleozoic continental margin of southwestern Gondwana, extending from northern Patagonia to northern Chile (Sato et al., 2015, and references therein). In the central region of northern Patagonia, plutonic and volcanic rocks, collectively known as the Los Menucos and La Esperanza complexes, are extensively exposed (Llambías and Rapela, 1984; Luppo et al., 2018, and references therein) (Fig. 10; Table 2). Luppo et al. (2018) compiled the available geochronologic data of this magmatic belt and suggested a main phase of granitoid intrusion and lava extrusion that spans ca. 245–270 Ma (Early Triassic–Middle Permian). Due to the widespread distribution of this magmatism in northern Patagonia, these authors even suggested that the Los Menucos and La Esperanza complexes could be regarded as a separate magmatic event from the Choiyoi province, with a probable peak of magmatism around the Permian–Triassic boundary (Luppo et al., 2018). Early Permian rocks, in contrast, are uncommon in the North Patagonian Massif, except for a granite dated as 281 Ma near the town of Valcheta and granites with U-Pb ages of 290–295 Ma in the westernmost sector of the NPM (Fig. 10; Table 2). These older granites are presently exposed from Piedra del Águila to Río Chico and are grouped in the Río Chico Complex with a confirmed Late Permian age (Pankhurst et al., 2006).

Choiyoi granitoids, volcanics, and volcaniclastics also comprise part of the Neuquén Basin basement (Schiuma and Llambías, 2008). A few available ages from subsurface data show granitoids of 286 Ma in the south and ignimbrites dated as 246 Ma in the north (Schiuma and Llambías, 2008; Barrionuevo et al., 2013) (Fig. 10). Early Triassic to Middle Permian rocks are also found in the Chadileuvú Block, where outcrops of volcanic and pyroclastic units are patchy (Domeier et al., 2011; Sato et al. 2015). There, the Sierra Chica silicic volcanic complex has U-Pb ages ranging from 268 to 257 Ma (Fig. 10). In the Las Matras Block, farther to the north, Choiyoi-related volcanic and pyroclastic rocks are common, with U-Pb ages ranging from 276 to 261 Ma (Tickyj et al., 2010; Barrionuevo et al., 2013). In the Sierra de la Ventana Belt and Río de La Plata Craton, Early Triassic–Early Permian rocks are not present, with the exception of the Lopez Lecube syenite, which was dated as 258 Ma (Pankhurst et al., 2006) (Fig. 10).

5.2.2 Interpretation

The Early Triassic–Middle Permian (240–272 Ma) zircon population of the Pilmatué Member with a 245–255 Ma peak appears to have a clear affinity with the northern Patagonian Los Menucos and Esperanza complexes, but a subordinate provenance from the Chadileuvú Block can also be considered. Although similar-age rocks are located farther to the north in the Las Matras and the San Rafael Blocks, the paleogeographic reconstruction for the Pilmatué delivery system makes it difficult to postulate a main source from this northern region, especially for the proximal samples representing delta-plain to fluvial sediments (EM-1 and EM-2, Fig. 10).

The Early Permian age population (273–299 Ma) of the Pilmatué sandstones with the 280 Ma peak seems to be comparatively underrepresented in the present geochronological data from the areas surrounding the Neuquén Basin (Fig. 10), although the presently sparse 280–295 Ma granites located in the western sector of the NPM could have been the source for this age population. Early Permian ages are also found in the Choiyoi basement of the Neuquén Basin, but these plutonic and volcanic rocks were subsequently covered by synrift and postrift sedimentary successions several thousands of meters thick (Howell et al., 2005) and thus were not exposed when the Pilmatué sediments were being deposited. The relative increase in Permian zircon grains in the distal samples (Fig. 8B) could be an indication of an additional contribution from the granites located in the westernmost sector of the North Patagonian Massif and thus reflecting the marine mixing of two different dispersal systems. According to Pankhurst et al. (2006), the emplacement of Permian magmatism began ca. 295 Ma and gradually moved toward the NE, which would explain the abundance of Early Permian (older) plutonic rocks in this western region. However, a catchment area located in the SW would also require a significant contribution from older Paleozoic rocks (Silurian to Carboniferous, see below), which is not recorded in the Pilmatué detrital-zircon age pattern (Fig. 8B). If both Permian and Paleozoic rocks were exposed in Early Cretaceous times, an alternative explanation would be that the Pilmatué source area did not extend into the North Patagonian Andes.

5.3 Silurian to Carboniferous (300–443 Ma) Sources

5.3.1 Potential Sources

Detrital-zircon grains from this population are very rare in the Pilmatué sandstones (Fig. 8). Devonian (390–401 Ma) and Carboniferous (ca. 320–330 Ma) plutonic rocks are presently exposed in the North Patagonian Andes, from San Martín de los Andes to El Bolsón (Fig. 10). The Devonian granitoids are attributed to magmatism and migmatization related to the Chanic orogenic belt that is well recorded in areas north of Patagonia (Hervé et al., 2018), whereas the early Carboniferous I-type granites were related to subduction and subsequent collision of the Deseado Massif with the North Patagonian Massif (Pankhurst et al., 2006).

5.3.2 Interpretation

The paleogeographic reconstruction proposed for the Pilmatué delivery system with predominant sediment flux from the east is consistent with the very low abundance of Devonian–Carboniferous zircon grains from these western Patagonian rocks, if they were exposed during the Early Cretaceous. Lower Permian granites contain zircon grains inherited from older rocks (namely from ca. 320 Ma, Pankhurst et al., 2006); so this could be an alternative origin for the few zircon grains present in the Pilmatué sandstones.

5.4 Ordovician (Ca. 450–490 Ma) Sources

5.4.1 Potential Sources

Detrital-zircon grains ranging from 450 to 490 Ma are relatively abundant in the Pilmatué sandstones, with a consistent peak ca. 460–475 Ma (Fig. 8). This period corresponds to Famatinian magmatism that extended from the Sierras Pampeanas north of the Neuquén Basin to the North Patagonia Massif south of the basin (Rapela et al., 2018, and references therein) (Fig. 1C). The Famatinian belt outcrops extensively in the Sierras Pampeanas due to Paleogene uplift. In contrast, Ordovician granites in the Chadileuvú Block and in the eastern sector of the NPM are represented by scattered and isolated exposures (Rapela et al., 2018) (Fig. 10). Early to Middle Ordovician meta-igneous rocks (465–475 Ma) are present in the central sector of the Chadileuvú Block (Chernicoff et al., 2010), whereas Early Ordovician plutonic rocks, having a consistent age of 475 Ma, are present in the south of the block (Pankhurst et al., 2014). In the eastern sector of the NPM, Early Ordovician granites (475–478 Ma) crop out in the Sierra Grande area, near the Atlantic coast (Rapela et al., 2018) (Fig. 10). Inland, in the Valcheta region (Fig. 10), Ar-Ar and K-Ar cooling ages for the Valcheta granites fall in the interval 430–470 Ma (Pankhurst et al., 2014, and references therein). Ordovician igneous rocks have not been documented from eastern Argentina (Sierra de la Ventana Belt and Rio de La Plata Craton) or from the

North Patagonian Andes (Fig. 10). Aside from igneous rocks, in the Sierra Grande area the iron-bearing, siliciclastic-dominated marine unit known as the Sierra Grande Formation crops out (Spalletti, 1993) (Fig. 10). It is mostly assigned to the Silurian–Early Devonian, and its detrital-zircon age patterns show a low to moderate contribution of Ordovician recycled zircon grains having a peak in 470–480 Ma (Uriz et al., 2011). In the Chadileuvú Block, Cambrian carbonates of the Sand Jorge Formation and Permian sandstones of the Carapacha Formation are presently very discontinuously exposed (Llambías et al., 1996; Melchor, 1999). However, no detrital-zircon data are available for these units.

5.4.2 Interpretation

The Ordovician age population in the Pilmatué detrital-zircon grains seems to correlate well with the Early Ordovician Famatinian magmatism present in both the Chadileuvú Block and the eastern sector of the NPM. Therefore, based on age alone, either of these regions could have been potential provenance areas for the Pilmatué delivery system. Significantly, Rapela et al. (2018) reviewed the Famatinian magmatism along southern South America and showed that this magmatic event has a peak of emplacement of ca. 475–480 Ma, which strongly matches the peak defined in the Pilmatué zircon population. The relatively high abundance of the Ordovician population in the zircon distributions versus the present-day minimal extent of the igneous-related outcrops suggests that a contribution from recycled zircon grains provided by the denudation of sedimentary units (such as the Sierra Grande Formation) is possible, albeit hard to quantify. Alternatively, some of the Ordovician zircon grains could be present as inherited cores in the younger volcanic rocks.

5.5 Cambrian (510–540 Ma) Sources

5.5.1 Potential Sources

The Cambrian age population of the Pilmatué zircon grains is restricted to ca. 510–540 Ma (Fig. 8A) and is present as a consistent 10%–14% in all the samples (Fig. 8B). Plutonic rocks of this interval are well exposed all across the Sierras Pampeanas in north-central Argentina (Fig. 1C) and are collectively known as the Pampean magmatism (Rapela et al., 2007; Casquet et al., 2018, among others). Few other regions around the Neuquén Basin have evidence for Cambrian igneous rocks, and their exposures are even more aerially restricted than the Ordovician rocks (Fig. 10), but their presence is significant for evaluating provenance patterns in Early Cretaceous time.

Locations of Cambrian igneous outcrops are in northern Patagonia, the Chadileuvú Block, and the Sierra de la Ventana Belt. In northern Patagonia, near Nahuel Niyeu (Fig. 10), a small Cambrian granodiorite body of 522–529 Ma was identified (Tardugno Granodiorite, Rapalini et al., 2013; Pankhurst et al., 2014). In the Sierra Grande area, the Ordovician granites (Fig. 10) intrude a volcanic-sedimentary succession with low-grade metamorphism known as the El Jagüelito Formation. A recent thorough review with additional geochronological evidence (González et al., 2018, and references therein) indicates an Early–Middle Cambrian age for this unit with at least two stages of volcanism (ca. 515 and ca. 530 Ma). Therefore, Pilmatué Cambrian zircon grains could have been recycled from this metasedimentary unit and similar units exposed close to the Nahuel Niyeu region. The detrital-zircon pattern of the El Jagüelito Formation has an age population with a peak at ca. 533 Ma, while the Nahuel Niyeu Formation has a similar peak in ca. 526 Ma (Rapela and Pankhurst, 2020, and references therein) (Fig. 11B). Lower Cambrian recycled zircon grains are also common in the siliciclastic sandstones of the Sierra Grande Formation (Fig. 10), representing 10%–20% of the samples reported by Uriz et al. (2011).

In the northern sector of the Chadileuvú Block, there are poorly exposed mafic granitoids dated as 520–528 Ma, which intrude Neoproterozoic high-grade metasediments (Chernicoff et al., 2012). In the Sierra de la Ventana Belt, Cambrian granites formed the basement of the Paleozoic basin, and their reported ages vary from 524 to 531 Ma (Rapela et al., 2003) (Fig. 10). In the Western Saldania Belt of South Africa, Cambrian (S-type and I-type) granites are common (Kisters and Belcher, 2018) (Fig. 10). U-Pb zircon ages indicate granites ranging from 550 to 515 Ma, with a peak of plutonic activity between ca. 540 and 530 Ma (Farina et al., 2014; Kisters and Belcher, 2018). The orogeny responsible for the generation of the Saldania Belt is correlated to the Pampean orogeny recorded in Argentina (Rapela et al., 2007; Casquet et al., 2018).

5.5.2 Interpretation

Cambrian zircon grains in the Pilmatué sands could have derived from a vast region ranging from the Chadileuvú Block and Sierra de la Ventana Belt toward the northeast, to the eastern sector of the NPM in the southeast. Rapela and Pankhurst (2020) recently reviewed the extent of Cambrian magmatism in northeast Patagonia and inferred that a poorly exposed Early Cambrian basement could be a significant component of the middle continental crust beneath this region and its extension onto the continental shelf to the east. Thus, it is possible that a larger area of Cambrian igneous rocks, as well as middle Paleozoic sedimentary successions (namely the Sierra Grande Formation), could have been exposed during deposition of the Pilmatué sands in the Early Cretaceous. It is also worthwhile to note that this Cambrian source could have extended farther into mid-continent positions of the supercontinent of Gondwana, as evidenced by Cambrian igneous ages in the Saldania Belt of South Africa.

5.6 Neoproterozoic (Ca. 580–635 Ma) and Mesoproterozoic (Ca. 1000–1100 Ma) Sources

5.6.1 Potential Sources

The Pilmatué sandstones have two significant Proterozoic zircon populations that span ca. 580–635 Ma (Ediacaran) and ca. 1000–1100 Ma (Stenian), respectively (Figs. 8 and 11A). These age populations are found as detrital-zircon grains in Cambrian metasedimentary units (El Jagüelito and Nahuel

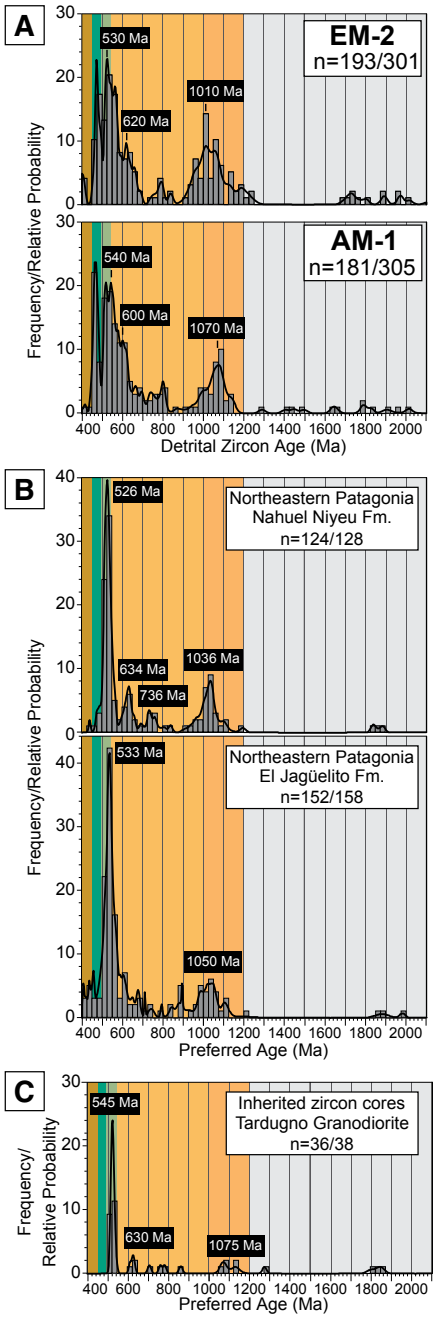

Figure 11. Comparison between Cambrian and Proterozoic detrital-zircon U-Pb age patterns of the Pilmatué Member and selected units of the eastern sector of the North Patagonian Massif. (A) Age probability diagrams and selected peaks for EM-2 and AM-1 samples of the Pilmatué Member. (B) Compilation of available data for the Nahuel Niyeu Formation and El Jagüelito Formation (compiled by Rapela and Pankhurst, 2020). (C) Inherited zircon core ages from the Cambrian Tardugno Granodiorite (Pankhurst et al., 2014).

Niyeu Formations) and middle Paleozoic sedimentary successions (Sierra Grande Formation), located in the eastern sector of the NPM (Fig. 10). The El Jagüelito Formation has a small population of Neoproterozoic grains and also Mesoproterozoic ages with a peak at 1050 Ma, while the Nahuel Niyeu Formation has remarkably similar age peaks in its Neoproterozoic (635 Ma) and Mesoproterozoic (1036 Ma) populations (Rapela and Pankhurst, 2020) (Fig. 11B). The Proterozoic detrital-zircon pattern for the Silurian–Devonian Sierra Grande Formation also mimics the pattern identified for the Nahuel Niyeu Formation (620 and 1050 Ma, Pankhurst et al., 2014) (Fig. 10).

Additionally, inherited zircon cores found in Cambrian, Ordovician, and Permian granites of the eastern sector of the NPM also have similar Neoproterozoic and Mesoproterozoic ages (Fig. 10). For example, the Cambrian Tardugno Granodiorite has zircon cores with peaks at 545, 630, and 1075 Ma (Pankhurst et al., 2014; Rapela and Pankhurst, 2020) (Fig. 11C), and the Permian Navarrete granite has inherited cores with ages of ca. 650 and ca. 1000 Ma (Pankhurst et al., 2006). Farther to the north, it has been demonstrated that sedimentary protoliths of the Sierras Pampeanas (Fig. 1C) are dominated by Neoproterozoic (broadly ca. 610–630 Ma) and late Mesoproterozoic (ca. 1000–1080 Ma) zircon grains, for example, in the Puncoviscana Formation (Rapela et al., 2007, 2011). Ediacaran–Early Cambrian low-grade metasedimentary rocks with similar zircon age patterns are also found in the Saldania Belt (Malmesbury Group, Casquet et al., 2018) (Fig 10); dominant age populations fall within 580–700, 700–960 Ma, and 960–1100 Ma (Frimmel et al., 2013). The single Proterozoic igneous rocks within the study region are found in the Sierra de la Ventana Belt (Fig. 10) and are represented by a limited outcrop of a granite that provided an Ediacaran age (607 Ma; Rapela et al., 2003).

5.6.2 Interpretation

The Neoproterozoic and Mesoproterozoic age populations of the Pilmatué sandstones could have been derived from denudation of the metasedimentary and sedimentary units (El Jagüelito, Nahuel Niyeu, and Sierra Grande Formations), as well as from inherited zircon grains within various younger magmatic rocks that occur in several regions of the eastern sector of the North Patagonian Massif. A single provenance from the granitoids of Sierra de la Ventana Belt would fail to explain the Mesoproterozoic population, but they could have provided some of the Ediacaran zircon grains. A contribution from more distant areas to the east, namely the Saldania Belt, also cannot be completely ruled out.

6. DISCUSSION

6.1 Remote versus Nearby Source Areas

This study presents the first detrital-zircon U-Pb ages of the Pilmatué Member (of the Agrio Formation), which represents deposition from the late Valanginian to the early Hauterivian in the Neuquén Basin (Fig. 12A). Previous data from the Agrio Formation is restricted to Tunik et al. (2010), who presented data from the late Hauterivian Avilé Member (Fig. 12B). Our findings suggest that Triassic–Permian age populations of the Pilmatué Member were probably sourced from the western sector of the North Patagonian Massif, whereas Early Jurassic, Cambrian, and Ordovician source rocks were most likely sourced from its eastern sector, with subordinate contributions from the Chadileuvú Block, the Sierra de la Ventana Belt, and probably the Saldania Belt (Figs. 10 and 12A).

Tunik et al. (2010) reported detrital-zircon ages from two samples of the Avilé Member (Fig. 12B), the sand-prone continental unit that overlies the Pilmatué Member and that developed after

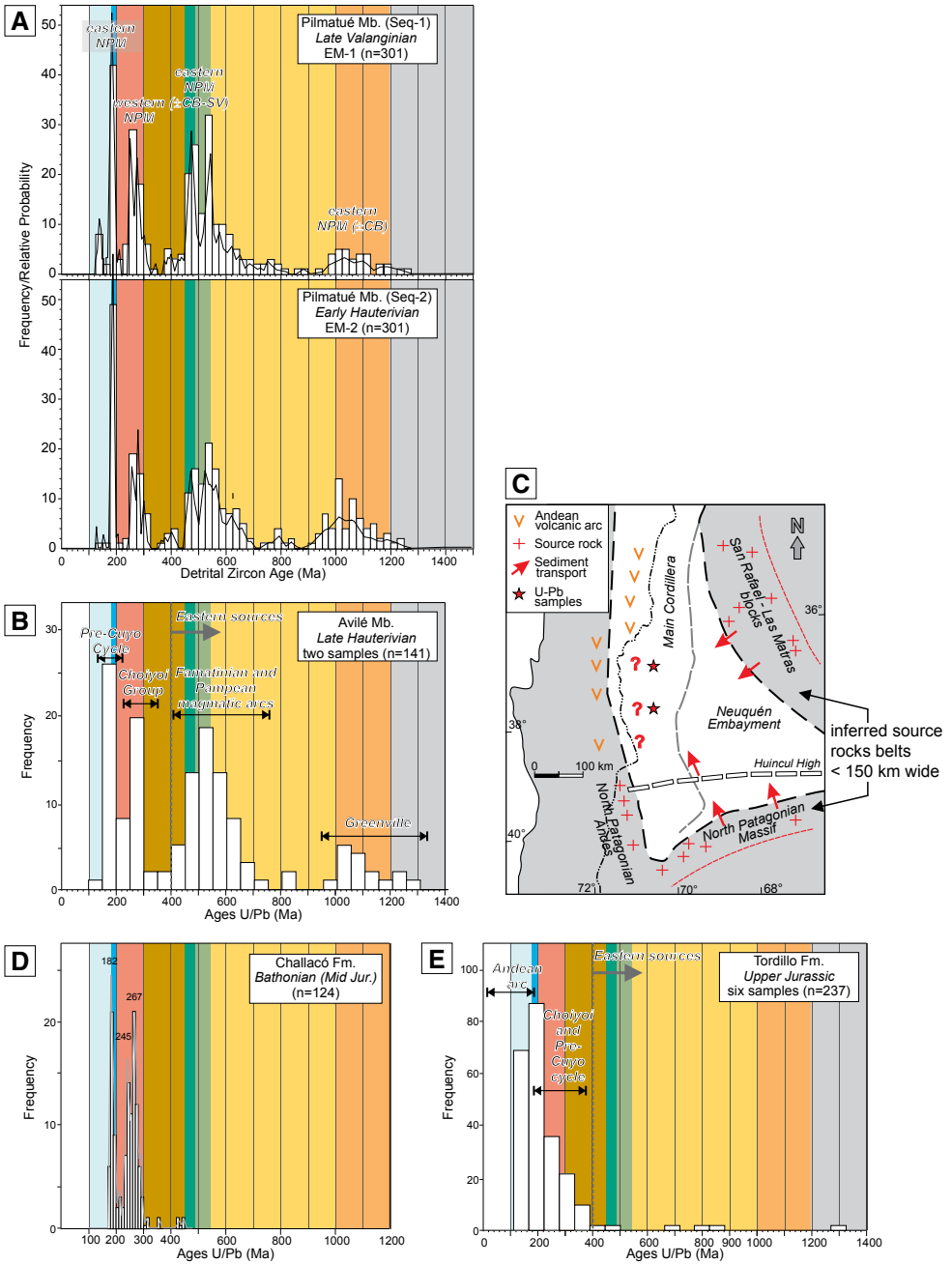

Figure 12. Detrital-zircon age distributions of late Valanginian (EM-1) and early Hauterivian (EM-2) samples of the Pilmatué Member of the Agrio Formation (A), and its comparison with other stratigraphic intervals of the basin. (B) The overlying late Hauterivian Avilé Member has similar age distributions (after Tunik et al., 2010), but the interpretation of source rocks provided by the authors is significantly different (see text for discussion). (C) Paleogeographic map with potential source regions for the Agrio Formation, based on that data (after Naipauer and Ramos, 2016). Note that contrary to this contribution, significant sediment supply is inferred coming from the San Rafael and Las Matras blocks, and the source-rock belts are mapped as narrow belts less than 150 km wide. (D) Detrital-zircon ages obtained from Middle Jurassic strata of southern Neuquén Basin (Challacó Formation), reported by Naipauer et al. (2018). Note the absence of Ordovician zircon grains and older, suggesting a rather uniform source area. (E) Detrital-zircon ages obtained from Upper Jurassic strata (Tordillo Formation) across the Main Cordillera (Naipauer and Ramos, 2016). Because this interval is associated with significant uplift and tectonic inversion, a predominant arc-derived provenance is postulated (Naipauer et al., 2014; Naipauer and Ramos, 2016). Mb—Member.

a dramatic base-level fall and disconnection with the proto–Pacific Ocean (Veiga et al., 2011) (Fig. 3A). Tunik et al. (2010), and subsequently Naipauer et al. (2014) and Naipauer and Ramos (2016), reviewing the same data set, assigned the prominent Early Jurassic peak in those data as representing provenance from synrift volcanic rocks within the Neuquén Basin (Precuyano Cycle). They also recognized prominent Triassic–Permian and Ordovician–Neoproterozoic age populations that they interpreted as reflecting sediment flux from the basement of the Neuquén Basin (Choiyoi Group) and from eastern foreland cratonic regions related to the Grenville, Pampean, and Famatian magmatic arcs (Fig. 12B). Their paleogeographic reconstructions for the Avilé Member commonly show sediment dispersal from the Sierra Pintada (San Rafael) and/or Las Matras blocks and from the central sector of the North Patagonian Massif (Fig. 12C). Although not specifically stated, these source areas were usually visualized as narrow regions not wider than 150 km.

The age populations defined for both the late Valanginian an early Hauterivian samples of the Pilmatué Member are remarkably similar to the late

Hauterivian Avilé zircon patterns (compare Figs. 12A and 12B). A key difference is the interpreted origin for the provenance of the Early Jurassic age population (175–190 Ma). A Precuyano cycle provenance for the Pilmatué Member age population is here discarded based on the fact that these synrift volcanic rocks were covered by hundreds of meters of postrift sedimentary strata by the time of Pilmatué accumulation (Howell et al., 2005; Iñigo et al., 2018). A western provenance from the North Patagonian Andes (Subcordilleran belt) is also dismissed for the Pilmatué sandstone based on the regional paleogeographic reconstruction demonstrating sediment dispersal from the southeast (Fig. 6) and the lack of a significant Devonian–Carboniferous zircon population that would have been derived from the southwest (Fig. 8). Late Paleozoic plutonic rocks are widespread in the western sector of the North Patagonian Massif (Fig. 10). Provenance from the Sierra Pintada–Las Matras blocks can also be ruled out because Early Jurassic rocks are not present there, and based on detailed sedimentologic studies, the main delivery system of the Pilmatué sands was located much farther to the south.

Additional evidence that supports a northeastern Patagonian provenance for the Early Jurassic age populations was indirectly provided by Naipauer et al. (2018). They reported U-Pb detrital-zircon patterns (Fig. 12D) and Hf isotope data from Middle Jurassic strata in the southern Neuquén Basin (Challacó Formation) and found consistent negative εHf values (–15.5 to –0.7) for a population of detrital-zircon grains ranging from 177 to 182 Ma, suggesting strong crustal contamination. Based on that evidence, Naipauer et al. (2018) concluded that these zircon grains were most probably derived from rhyolitic volcanic rocks presently exposed solely in the eastern sector of the NPM and highlighted the potential role that the Marifil Complex could have had as a major source of clastics to the Jurassic sediments of the Neuquén Basin. Therefore, both remote and relatively nearby source areas such as Huincul-related intra-basinal highs and the western magmatic arc would have been providing sediment to the basin during Middle Jurassic time (Naipauer and Ramos, 2016; Pujols et al., 2018).

The eastern sector of the North Patagonian Massif appears to continue beneath the Argentine shelf as evidenced by similar geophysical attributes and NNW-oriented fabrics (Max et al., 1999; Pángaro and Ramos, 2012). Moreover, Lovecchio et al. (2019, their fig. 2) recently suggested that the Early Jurassic Chon Aike magmatic province could have extended to the North Malvinas Basin, likely located a few hundreds of kilometers from the present-day Atlantic Patagonian coastline. So the major source region for the Pilmatué sands could have easily extended to the eastern margin of Argentina, located at least 250 km to the east of Peninsula Valdés (Fig. 10). Importantly, however, the Saldania Belt in southern South Africa is also dominated by Neoproterozoic (Ediacaran) metasedimentary units intruded by Cambrian granites (Fig. 10), which together contain all the same ages that are present in the Pilmatué detrital-zircon grains. According to Pángaro and Ramos (2012, their fig. 14), the Saldania Belt was located ~600 km east of the Peninsula Valdés in Valanginian–Hauterivian times, just before Atlantic break-up at this latitude. So, in a Gondwana-scale perspective, it could be possible that the source areas of the Pilmatué sands extended ~1000 km east into the mid-continent region of Gondwana.

From the sedimentological point of view, one of the more striking features of the Pilmatué Member is that the maximum grain size is never coarser than lower medium sand (0.30 mm), although the proportion of sand varies from ~80% in the proximal regions (El Mangrullo field) to 10% or less in distal regions (Fig. 4). A hundred kilometers to the east, where the unit becomes fully fluvial and is called Lower Centenario Member (Centenario hydrocarbon field, Fig. 1C), the dominant grain size is consistently medium and coarse (Digregorio, 1972; Schwarz et al., 2019). Therefore, the Pilmatué sands, which were accumulated in ~2.8–3.0 m.y. and are distributed across more than 40,000 km² (Fig. 6), were probably fed by a delivery system long enough to be able to sort the different grain sizes and with a catchment area large enough to constantly supply substantial volumes of siliciclastics to the marine system. Veiga et al. (2019) related the total detrital volume produced in 3 m.y. with sediment supply equations to estimate that the size of the catchment area for the Pilmatué-Centenario delivery system would be more than ten times the size of the total marine depocenter (a minimum size of ~1,000,000 km²). This vast sediment source region agrees with source areas for the Pilmatué sands located as far as 1000 km from the coeval shoreline.

6.2 Pilmatué Sands: The End of a Long-Lived Delivery System in SW Gondwana?

Sedimentary basins located at the margins of continents act as the final base level for mid-continent regions that are sometimes located thousands of kilometers away from the basin (e.g., Latrubesse, 2015). This condition of exceptionally long sediment transfer zones is probably reinforced in supercontinents. For example, the Late Paleozoic Karoo Basin of southern Pangea has been proposed as the final repository of clastic detritus mostly denuded from plutonic and volcanic rocks of the Choiyoi group presently located in western Argentina and Chile (Johnson, 1991; Van Lente, 2004; Sato et al., 2015; Gomis-Cartesio et al., 2018). This would imply a delivery system running from west to east across southern Pangea over 1500 km. Unsurprisingly, the clastic sediments that reached the marine realm and eventually the deep-water settings were fine-grained sand or finer caliber (e.g., Hodgson et al., 2006; Gomis-Cartesio et al., 2018). Nonetheless, the large supply of sediments was enough to build a long-term progradational system from fluvial to deep-water to fluvial deposits (Hodgson et al., 2006); this system is more than 3500 m thick. Although the age of this Permian–Triassic progradational succession (Ecca and Beaufort Groups) is not well constrained, it would have endured for ~40 m.y. (from ca. 290–253 Ma according to Sato et al., 2015, and discussions therein). This Patagonian–South African source-to-sink delivery system would have been not only vast but also long lasting.

The marine Neuquén Basin clearly acted as a base level for southwestern Gondwana delivery systems during the Jurassic and Early Cretaceous (Macdonald et al., 2003), but it was not connected continuously with the proto–Pacific Ocean. During

episodes of major tectonic uplift and arc growth, there was complete disconnection from the adjacent ocean and onset of fully continental depositional systems with significant clastic volume provided by local sources with abundant coarse gravel to coarse sand deposited in alluvial settings. The Kimmeridgian Tordillo Formation represents one of these intervals (Fig. 2), and detrital-zircon grains from this unit show a dominance of arc-derived provenance (Naipauer et al., 2014; Naipauer and Ramos, 2016) (Fig. 12E) that clearly contrasts with the Agrio zircon patterns reported from the Pilmatué and Avilé members (Figs. 12A and 12B).

The Pilmatué Member strata and their detrital-zircon grains represent a time of relative tectonic quiescence (Vergani et al., 1995) and long-term progradation dominated by fine sand or finer sediments (Schwarz et al., 2018a, 2018b; Schwarz et al., 2019). We propose that there was a main delivery system with an elongated geometry bringing clastic sediment from mid-continent regions of southern Gondwana at that time (Fig. 13). Along the way, the system was effective at sorting and therefore transported and deposited only fine-grained sands in the distal segment of the system found in the Neuquén Basin. The elongated catchment area had a complex geological composition, including Lower Jurassic volcanic rocks, Triassic to Permian igneous rocks, and Lower Paleozoic to Neoproterozoic plutonic, volcanic, and metasedimentary rocks (Fig. 13). These detrital materials were mostly eroded from the eastern and western sectors of the North Patagonian Massif and its eastern continuation beneath the Argentine continental shelf, but probably also from some regions in the present Chadileuvú Block and Sierra de la Ventana Belt, which were probably positive topographic features during Early Cretaceous times (Pángaro and Ramos, 2012), and thus limiting the northern extension of this vast delivery system (Fig. 13).

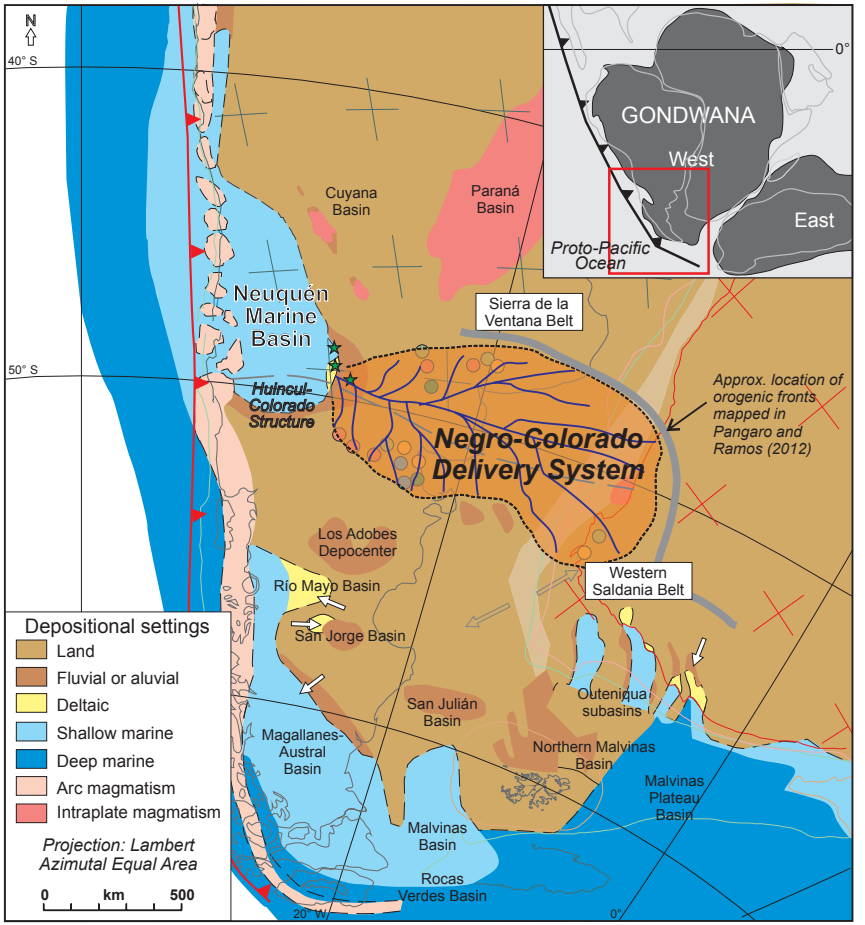

Figure 13. Proposed reconstruction of the Negro-Colorado Delivery System that fed the Pilmatué sands in the Neuquén Basin, projected onto a paleogeographic reconstruction of southwestern Gondwana at ca. 135 Ma (modified from Macdonald et al., 1993). Dots represent present outcropped rocks with known ages to the east of the Neuquén Basin (colors as in Fig. 10). The axis of this system could have approximately correlated with the Huincul-Colorado line, whereas the extension of the catchment area could have been limited by orogenic fronts, to the north by the Sierra de la Ventana Belt, and to the east by the Saldania Belt. Green stars show the relative position of the samples.

The geographic location of this Valanginian–Hauterivian longitudinal delivery system approximately correlates with several key features in southern South America. The Negro River valley, the largest river in Patagonia (in relation to flow rate), runs eastwards from the Andes to the South Atlantic Ocean and occupies a similar location as the proposed Pilmatué system (Figs. 1A and 10). In addition, the inferred location runs subparallel to the Huincul-Colorado structure (Macdonald et al., 2003) or Huincul fault zone (Gregori et al., 2008), which represents a first-order geological and morphological feature of present South America (Fig. 13). This geological structure holds key components of the history of the Neoproterozoic to Early Cambrian amalgamation of southwest Gondwana (Gregori et al., 2008; Rapalini et al., 2013; Pankhurst et al., 2014). The inferred delivery system probably would have been located immediately to

the north of the Huincul fault zone (Fig. 13). The proposed delivery system also correlates approximately with the elongation of the offshore Colorado Basin (Fig. 1C), which after several Jurassic syn-rift episodes characterized by small-scale grabens, eventually became a larger basin post–break-up of the South Atlantic in Barremian–Albian time (Macdonald et al., 2003; Lovecchio et al., 2018). Thus, this delivery system appears to have been a significant, long-lasting geomorphological feature in southwest Gondwana and is herein termed the Negro-Colorado Delivery System.

The Early to Middle Jurassic Cuyo Group succession (Toarcian–Callovian) of the Neuquén Basin has recently been the focus of basin-scale studies combining extensive 3D seismic-reflection and well data (Brinkworth et al., 2018). Beginning with the Toarcian strata, this up to 1000-m-thick succession shows a consistent and long-lived entry point located around Neuquén city and a clear clinoform progradation from southeast to northwest. From Late Toarcian–Aalenian and onwards, an additional entry point is identified in the northeast sectors of the basin. As previously mentioned, detrital-zircon patterns and Hf isotope signatures found in the partially coeval succession exposed in the southern Neuquén Basin (Fig. 12D) allowed Naipauer et al. (2018) to highlight that the northeastern Patagonian region was clearly an active source (albeit not the only one, cf. Pujols et al., 2018) for fluvial and coeval marine sediments since the early development of the basin in the Toarcian (Los Molles Formation), and it was still active some 20 m.y. later during the Bathonian (Challacó Formation, Fig. 2).

Together, these pieces of evidence suggest that the Negro-Colorado Delivery System was not only a continental-scale system, but a long-lived one, which was responsible for (and related to) denudation, erosion, and transport of clastics across a large region of southwestern Gondwana from the Early Jurassic to Early Cretaceous, a timespan of ~60 m.y. Similar long-lived, large-scale systems are known from other regions. For example, the paleo–Orange river in South Africa is thought to have formed a paleodelta that was established ca. 103 Ma and existed to ca. 60–70 Ma (Bluck et al., 2007). This drainage system, with an area of ~900,000 km^2, represents the main sediment outfall for southern Africa (Bremner et al., 1990). In North America, several detrital-zircon studies have now demonstrated far-flung sediment delivery systems that spanned the entire width of the continent during the peak assembly of the Pangean supercontinent (Pennsylvanian–Permian) (Gehrels et al., 2011; Kissock et al., 2017; Thomas et al., 2020), and the same would remain true for the source-to-sink delivery system that would have connected Patagonian source rocks with the Karoo basin during the late Paleozoic (Johnson, 1991; Sato et al., 2015; Gomis-Cartesio et al., 2018).

Significantly, by tracking the detrital-zircon grain patterns of sand reaching the Neuquén Basin through the Negro-Colorado Delivery System, it is possible to reconstruct the denudation history of its geological substrate though time. The Early and Middle Jurassic sandstones lack detrital-zircon grains from Ordovician and older rocks that are so common in the Lower Cretaceous Pilmatué and Avilé Members (compare Figs. 12A and 12E). This could suggest a relatively simple source area composition in northeastern Patagonia for the Early Jurassic, largely dominated by the almost coeval Marifil rhyolitic extensive extrusive complex and the Permian–Triassic igneous rocks of the Choiyoi group. By the late Valanginian–early Hauterivian (132–129 Ma), large volumes of the Jurassic rocks could have been eroded from the source area and transferred to the Neuquén Basin, leaving exhumed a more complex source composition with Ordovician, Cambrian, and Proterozoic igneous, sedimentary, and metamorphic rocks. Because this time approximately matches the break-up and opening of the South Atlantic Ocean at these latitudes (Macdonald et al., 2003; Lovecchio et al., 2018; Will and Frimmel, 2018), the Gondwana-scale, Negro-Colorado Delivery System, which probably transferred clastics from present Africa all the way to present Chile for ~60 m.y., finally would have come to an end.

7. CONCLUSIONS

This contribution provides the first detailed detrital-zircon U-Pb geochronology of sand-prone deposits associated with distributary channels, mouth bars (of delta-front settings), and shoreface settings of the late Valanginian–early Hauterivian Pilmatué Member in the Neuquén Basin (southwestern Gondwana) for a better understanding of far-flung versus local fluvial delivery systems to the basin. The basin-scale reconstructed paleogeography of the unit is characterized by a clear proximal-distal trend, ranging from delta-plain and/or fluvial settings in the southeast grading to delta-front and/or shoreface and prodelta and/or offshore environments in the west and northwest. Delta-plain and fluvial deposits are dominated by medium- and fine-grained sandstones, whereas sand-rich, shallow-marine deposits are characterized by fine to very fine-grained sandstones. Detrital-zircon analysis suggests that Triassic–Permian age populations of the Pilmatué Member were probably sourced from the western sector of the North Patagonian Massif, whereas Early Jurassic, Cambrian, Ordovician, and Proterozoic source rocks were most likely located in the eastern sector of the North Patagonian Massif, with subordinate contributions from the Chadileuvú Block, the Sierra de la Ventana Belt, and probably the Saldania Belt in southernmost Africa. We thus propose that the source areas of the Pilmatué sands extended ~1000 km east of their final repositories and that a long-lasting fluvial system, here called Negro-Colorado Delivery System, was responsible for (and related to) denudation, erosion, and transport of clastics across a large region of southwestern Gondwana.

ACKNOWLEDGMENTS

The authors thank Pampa Energia S.A. for providing the core sample material. Consejo Nacional de Investigaciones Científicas y Técnicas (CONICET) and Universidad Nacional de La Plata are acknowledged for partially supporting this project. University of Iowa undergraduate Ben Howard assisted with mineral separation. Support for the Arizona LaserChron Center is provided by National Science Foundation grant EAR-1649254. The manuscript benefited from constructive reviews by J. Fodsick and two anonymous reviewers, as well as additional comments by Associate Editor C. Spencer.

REFERENCES CITED

Aguirre-Urreta, B., Lazo, D.G., Griffin, M., Vennari, V., Parras, A.M., Cataldo, C., Garberoglio, R., and Luci, L., 2011, Megainvertebrados del Cretácico y su importancia bioestratigráfica,

in Leanza, H.A., Arregui, C., Carbone, O., Danielli, J.C., and Vallés, J.M., eds., Geología y Recursos Naturales de la Provincia del Neuquén, 18° Congreso Geológico Argentino, Argentina: Asociación Geológica Argentina, p. 465–488.

Aguirre-Urreta, B., Lescano, M., Schmitz, M.D., Tunik, M., Concheyro, A., Rawson, P.F., and Ramos, V.A., 2015, Filling the gap: New precise Early Cretaceous radioisotopic ages from the Andes: Geological Magazine, v. 152, p. 557–564, https://doi.org/10.1017/S001675681400082X.

Aguirre-Urreta, B., Schmitz, M., Lescano, M., Tunik, M., Rawson, P.F., Concheyro, A., Buhler, M., and Ramos, V.A., 2017, A high precision U-Pb radioisotopic age for the Agrio Formation, Neuquén Basin, Argentina: Implications for the chronology of the Hauterivian Stage: Cretaceous Research, v. 75, p. 193–204, https://doi.org/10.1016/j.cretres.2017.03.027.

Aguirre-Urreta B., Martinez, M., Schmitz, M., Lescano, M., Omarini, J., Tunik, M., Kuhnert, H., Concheyro, A., Rawson, P.F., Ramos, V.A., Reboulet, S., Noclinh, N., Frederichs, T., Nickl, A., and Pälike, H., 2019, Interhemispheric radio-astrochronological calibration of the time scales from the Andean and the Tethyan areas in the Valanginian–Hauterivian (Early Cretaceous): Gondwana Research, v. 70, p. 104–132, https://doi.org/10.1016/j.gr.2019.01.006.

Aguirre-Urreta, M.B., Rawson, P.F., Concheyro, G.A., Bown, P.R., and Ottone, E.G., 2005, Lower Cretaceous (Berriasian-Aptian) biostratigraphy of the Neuquén Basin, *in* Veiga, G.D., Spalletti, L.A., Howell, J.A., and Schwarz, E., eds., The Neuquén Basin: A Case Study in Sequence Stratigraphy and Basin Dynamics: Geological Society of London Special Publication 252, p. 57–81, https://doi.org/10.1144/GSL.SP.2005.252.01.04.

Alric, V, Haller, M., Féraud, J., Bertrand, H., and Zubia, M., 1996, Cronología ^{40}Ar-^{39}Ar del volcanismo jurásico de la Patagonia extrandina. Buenos Aires, Actas 13° Congreso Geológico Argentino and 3° Congreso de Exploración de Hidrocarburos, v. 5, p. 243–250.

Argüello Scotti, A., and Veiga, G.D., 2019, Sedimentary architecture of an ancient linear megadune (Barremian, Neuquén Basin): Insights into the long-term development and evolution of aeolian linear bedforms: Sedimentology, v. 66, p. 2191–2213, https://doi.org/10.17605/OSF.IO/6H7EN.

Barrionuevo, M., Arnosio, M., and Llambías, E.J., 2013, Nuevos datos geocronológicos en subsuelo y afloramientos del Grupo Choiyoi en el oeste de La Pampa: Implicancias estratigráficas: Revista de la Asociación Geológica Argentina, v. 70, p. 31–39.

Bluck, B.J., Ward, J.D., Cartwright, J., and Swart, R., 2007, The Orange River, southern Africa: An extreme example of a wave-dominated sediment dispersal system in the South Atlantic Ocean: Journal of the Geological Society of London, v. 164, p. 341–351, https://doi.org/10.1144/0016-76492005-189.

Bremner, J.M., Rogers, J., and Willis, J.P., 1990, Sedimentological aspects of the 1988 Orange River floods: Transactions of the Royal Society of South Africa, v. 47, p. 247–294, https://doi.org/10.1080/00359199009520243.

Brinkworth, W., Vocaturo, G., Loss, L., Giunta, D., Mortaloni, E., and Massaferro, J.L., 2018, Estudio cronoestratigráfico y evolución paleoambiental del Jurásico Inferior-Medio en el Engolfamiento de la Cuenca Neuquina, Argentina, *in* Gardini, M., Gómez, M., Manceda, R., Ayoroa, M.A., Limeres, M., Peroni, G., Cruz, C.E., Malone, P., and Villar, H., eds., Sesiones Generales, 10° Congreso de Exploración y Desarrollo de Hidrocarburos, Mendoza, Argentina: Instituto Argentino del Petróleo, p. 597–621.

Burgess, P.M., Flint, S.S., and Johnson, S., 2000, Sequence stratigraphic interpretation of turbiditic strata: An example from Jurassic strata of the Neuquén basin, Argentina: Geological Society of America Bulletin, v. 112, p. 1650–1666, https://doi.org/10.1130/0016-7606(2000)112<1650:SSIOTS>2.0.CO;2.

Carbone, O., Franzese, J., Limeres, M., Delpino, D., and Martínez, R., 2011, El Ciclo Precuyano (Triásico Tardío-Jurásico Temprano) en la Cuenca Neuquina, *in* Leanza, H.A., Arregui, C., Carbone, O., Danielli, J.C., and Vallés, J.M., eds., Geología y Recursos Naturales de la Provincia del Neuquén, 18° Congreso Geológico Argentino, Argentina: Asociación Geológica Argentina, p. 63–76.

Casquet, C., Dahlquist, J.A., Verdecchia, S.O., Baldo, E.G., Galindo, C., Rapela, C.W., Pankhurst, R.J., Morales, M.M., Murra, J.A., and Fanning, C.M., 2018, Review of the Cambrian Pampean orogeny of Argentina: A displaced orogen formerly attached to the Saldania Belt of South Africa?: Earth-Science Reviews, v. 177, p. 209–225, https://doi.org/10.1016/j.earscirev.2017.11.013.

Chemale, F., Scheepers, R., Gresse, P.G., and Schmus, W.R.V., 2011, Geochronology and sources of late Neoproterozoic to Cambrian granites of the Saldania Belt: International Journal of Earth Sciences, v. 100, p. 431–444, https://doi.org/10.1007/s00531-010-0579-1.

Chernicoff, C.J., Zappettini, E.O., Santos, J.O.S., Allchurch, S., and McNaughton, N.J., 2010, The southern segment of the Famatinian magmatic arc, La Pampa Province, Argentina: Gondwana Research, v. 17, p. 662–675, https://doi.org/10.1016/j.gr.2009.10.008.

Chernicoff, C.J., Zappettini, E.O., Santos, J.O.S., Godeas, M.C., Belousova, E., and McNaughton, N.J., 2012, Identification and isotopic studies of early Cambrian magmatism (El Carancho Igneous Complex) at the boundary between Pampia terrane and the Rio de la Plata craton, La Pampa province, Argentina: Gondwana Research, v. 21, p. 378–393, https://doi.org/10.1016/j.gr.2011.04.007.

Cobbold, P.R., and Rossello, E.A., 2003, Aptian to recent compressional deformation of the Neuquén Basin, Argentina: Marine and Petroleum Geology, v. 20, p. 429–443, https://doi.org/10.1016/S0264-8172(03)00077-1.

Da Silva, L.C., Gresse, P.G., Scheepers, R., McNaughton, N.J., Hartmann, L.A., and Fletcher, I., 2000, U-Pb and Sm-Nd age constraints on the timing and sources of the Pan-African Cape Granite Suite, South Africa: Journal of African Earth Sciences, v. 30, p. 795–815, https://doi.org/10.1016/S0899-5362(00)00053-1.

Digregorio, J.H., 1972, Neuquén, *in* Leanza, A.F., ed., Geología Regional Argentina, Córdoba, Argentina: Academia Nacional de Ciencias de Córdoba, p. 439–506.

Domeier, M., Van der Voo, R., Tohver, E., Tomezzoli, R.N., Vizan, H., and Kirshner, J., 2011, New Late Permian paleomagnetic data from Argentina: Refinement of the apparent polar wander path of Gondwana: Geochemistry, Geophysics, Geosystems, v. 12, https://doi.org/10.1029/2011GC003616.

Domínguez, R.F., and Di Benedetto, M., 2018, Casos de variabilidad lateral en el sistema Vaca Muerta-Quintuco y su impacto en la distribución de facies ricas en materia orgánica, *in* Santiago, M., Fantín, M., Vallejo, M.D., González Tomassini, F., Estrada, S., Marchal, D., Aguirre, H., and López, S., eds., Simposio de Recursos No Convencionales: Hacia una Nueva Convención, 10° Congreso de Exploración y Desarrollo de Hidrocarburos, Mendoza, Argentina: Instituto Argentino del Petróleo, p. 91–104.

Farina, F., Stevens, G., Gerdes, A., and Frei, D., 2014, Small-scale Hf isotopic variability in the Peninsula pluton (South Africa): The processes that control inheritance of source ^{176}Hf/^{177}Hf diversity in S-type granites: Contributions to Mineralogy and Petrology, v. 168, 1065, https://doi.org/10.1007/s00410-014-1065-8.

Franzese, J.R., and Spalletti, L.A., 2001, Late Triassic–early Jurassic continental extension in southwestern Gondwana: Tectonic segmentation and pre-break-up rifting: Journal of South American Earth Sciences, v. 14, p. 257–270, https://doi.org/10.1016/S0895-9811(01)00029-3.

Franzese, J.R., Veiga, G.D., Schwarz, E., and Gómez-Pérez, I., 2006, Tectono-stratigraphic evolution of a Mesozoic rift border system: The Chachil depocentre, southern Neuquén Basin, Argentina: Journal of the Geological Society of London, v. 163, p. 707–721, https://doi.org/10.1144/0016-764920-082.

Frimmel, H.E., Basei, M.A.S., Correa, V.X., and Mbangula, N., 2013, A new lithostratigraphic subdivision and geodynamic model for the Panafrican western Saldania Belt, South Africa: Precambrian Research, v. 231, p. 218–235, https://doi.org/10.1016/j.precamres.2013.03.014.

Gehrels, G., 2012, Detrital Zircon U-Pb Geochronology: Current Methods and New Opportunities, *in* Busby, C., and Azor, A., eds., Tectonics of Sedimentary Basins: Recent Advances: Chichester, Wiley-Blackwell Publishing, p. 45–62, https://doi.org/10.1002/9781444347166.ch2.

Gehrels, G., Valencia, V., and Pullen, A., 2006, Detrital Zircon Geochronology by Laser Ablation Multicollector ICPMS at the Arizona LaserChron Center, *in* Olszewski, T., ed., Geochronology: Emerging Opportunities: Paleontology Society Papers, Volume 12, p. 67–76, https://doi.org/10.1017/S1089332600001352.

Gehrels, G.E., Blakey, R., Karlstrom, K.E., Timmons, J.M., Dickinson, B., and Pecha, M., 2011, Detrital zircon U-Pb geochronology of Paleozoic strata in the Grand Canyon, Arizona: Lithosphere, v. 3, no. 3, p. 183–200, https://doi.org/10.1130/L121.1.

Gomis-Cartesio, L.E., Poyatos-Moré, M., Hodgson, D.M., and Flint, S.S., 2018, Shelf-margin clinothem progradation, degradation and readjustment: Tanqua depocentre, Karoo Basin (South Africa): Sedimentology, v. 65, p. 809–841, https://doi.org/10.1111/sed.12406.

González, P.D., Sato, A.M., Naipauer, M., Varela, R., Basei, M., Sato, K., Llambías, E.J., Chemale, F., and Castro Dorado, A., 2018, Patagonia–Antarctica Early Paleozoic conjugate margins: Cambrian synsedimentary silicic magmatism, U-Pb dating of K-bentonites, and related volcanogenic rocks: Gondwana Research, v. 63, p. 186–225, https://doi.org/10.1016/j.gr.2018.05.015.

Gozálvez, M., 2009, Petrografía y edad ^{40}Ar-^{39}Ar de leucogranito peraluminosos al oeste de Valcheta. Macizo Nordpatagónico (RíoNegro): Revista de la Asociación Geológica Argentina, v. 64, p. 275–284.

Gregori, D.A., Kostadinoff, J., Strazzere, L., and Raniolo, A., 2008, Tectonic significance and consequences of the Gondwanide

orogeny in northern Patagonia, Argentina: Gondwana Research, v. 14, p. 429–450, https://doi.org/10.1016/j.gr.2008.04.005.

Hervé, F., Calderón, M., Fanning, C.M., Pankhurst, R.J., Rapela, C.W., and Quezada, P., 2018, The country rocks of Devonian magmatism in the North Patagonian Massif and Chaitenia: Andean Geology, v. 45, p. 301–317, https://doi.org/10.5027/andgeoV45n3-3117.

Hodgson, D.M., Flint, S.S., Hodgetts, D., Drinkwater, N.J., Johannessen, E.P., and Luthi, S.M., 2006, Stratigraphic evolution of fine-grained submarine fan systems, Tanqua Depocenter, Karoo Basin, South Africa: Journal of Sedimentary Research, v. 76, p. 20–40, https://doi.org/10.2110/jsr.2006.03.

Howell, J.A., Schwarz, E., Spalletti, L.A., and Veiga, G.D., 2005, The Neuquén Basin: An overview, *in* Veiga, G.D., Spalletti, L.A., Howell, J.A., and Schwarz, E., eds., The Neuquén Basin: A Case Study in Sequence Stratigraphy and Basin Dynamics: Geological Society of London Special Publication 252, p. 1–14.

Ibañez-Mejia, M., Pullen, A., Pepper, M., Urbani, F., Ghoshal, G., and Ibañez-Mejia, J.C., 2018, Use and abuse of detrital zircon U-Pb geochronology—A case from the Río Orinoco delta, eastern Venezuela: Geology, v. 46, p. 1019–1022, https://doi.org/10.1130/G45596.1.

Iñigo, J.F., Vargas, R., Novara, E., Pereira, D.M., and Schwarz, E., 2018, La Formación Loma Montosa en el borde nororiental de la Cuenca Neuquina: Análisis secuencial, caracterización paleoambiental y prospectividad remanente, *in* Gardini, M., Gómez, M., Manceda, R., Ayoroa, M.A., Limeres, M., Peroni, G., Cruz, C.E., Malone, P., and Villar, H., eds., Sesiones Generales, 10° Congreso de Exploración y Desarrollo de Hidrocarburos, Mendoza, Argentina: Instituto Argentino del Petróleo, p. 623–645.

Johnson, M.R., 1991, Sandstone petrography, provenance and plate tectonic setting in Gondwana context of the southeastern Cape-Karoo Basin: South African Journal of Geology, v. 94, p. 137–154.

Kissock, J.K., Finzel, E.S., Malone, D.H., and Craddock, J.P., 2017, Lower–Middle Pennsylvanian strata in the North American midcontinent record the interplay between erosional unroofing of the Appalachians and eustatic sea-level rise: Geosphere, v. 14, https://doi.org/10.1130/GES01512.1.

Kisters, A., and Belcher, R., 2018, The Stratigraphy and Structure of the Western Saldania Belt, South Africa and Geodynamic Implications, *in* Siegesmund, S., Basei, M.A.S., Oyhantçabal, P., and Oriolo, S., eds., Geology of Southwest Gondwana, Regional Geology Reviews: Cham, Springer International Publishing, p. 387–410, https://doi.org/10.1007/978-3-319-68920-3_14.

Latrubesse, E.M., 2015, Large rivers, megafans and other Quaternary avulsive fluvial systems: A potential "who's who" in the geological record: Earth-Science Reviews, v. 146, p. 1–30, https://doi.org/10.1016/j.earscirev.2015.03.004.

Lazo, D.G., and Damborenea, S.E., 2011, Barremian bivalves from the Huitrín Formation, West-Central Argentina: Taxonomy and paleoecology of a restricted marine association: Journal of Paleontology, v. 85, p. 719–743, https://doi.org/10.1666/10-098.1.

Lazo, D.G., Concheyro, G.A., Ottone, E.G., Guler, M.V., and Aguirre-Urreta, M.B., 2009, Bioestratigrafía integrada de la Formatión Agrio en su localidad tipo, Cretácico temprano de Cuenca Neuquina: Revista de la Asociación Geológica Argentina, v. 65, p. 322–341.

Lazo, D.G., Bressán, G.S., Schwarz, E., and Veiga, G.D., 2020, First articulated stalked crinoids from the Mesozoic of South America: Two new species from the Lower Cretaceous of the Neuquén Basin, west-central Argentina: Journal of Paleontology, v. 94, p. 716–733, https://doi.org/10.1017/jpa.2020.15.

Legarreta, L., and Uliana, M.A., 1991, Jurassic–Cretaceous marine oscillations and geometry of back-arc basin fill, Central Argentine Andes, *in* Macdonald, D.I., ed., Sedimentation, Tectonics and Eustasy: Sea Level Changes at Active Plate Margins: IAS Special Publication 12, p. 429–450.

Llambías, E.J., and Rapela, C.W., 1984, Geología de los complejos eruptivos del Paleozoico superior de La Esperanza, provincia de Río Negro: Revista de la Asociación Geológica Argentina, v. 39, p. 220–243.

Llambías, E.J., Melchor, R.N., Tickyj, H., and Sato, A.M., 1996, Geología del Bloque del Chadileuvú: Buenos Aires, Actas Congreso Geológico Argentino y 3° Congreso de Exploración de Hidrocarburos, v. 5, p. 417–425.

Lovecchio, J.P., Rohais, S., Joseph, P., Bolatti, N., Kress, P.R., Gerster, R., and Ramos, V.A., 2018, Multi-stage rifting evolution of the Colorado basin (offshore Argentina): Evidence for extensional settings prior to the South Atlantic opening: Terra Nova, v. 30, p. 359–368, https://doi.org/10.1111/ter.12351.

Lovecchio, J.P., Naipauer, M., Cayo, L.E., Rohais, S., Giunta, D., Flores, G., Gerster, R., Bolatti, N.D., Joseph, P., Valencia, V.A., and Ramos, V.A., 2019, Rifting evolution of the Malvinas basin, offshore Argentina: New constrains from zircon U-Pb geocrhonology and seismic characterization: Journal of South American Earth Sciences, v. 95, https://doi.org/10.1016/j.jsames.2019.102253.

Luci, L., and Lazo, D.G., 2015, Living on an island: Characterization of the encrusting fauna of large pectinid bivalves from the Lower Cretaceous of the Neuquén Basin, west-central Argentina: Lethaia, v. 48, p. 205–226, https://doi.org/10.1111/let.12100.

Luppo, T., López de Luchi, M.G., Rapalini, A.E., Martínez Dopico, C.I., and Fanning, C.M., 2018, Geochronologic evidence of a large magmatic province in northern Patagonia encompassing the Permian–Triassic boundary: Journal of South American Earth Sciences, v. 82, p. 346–355, https://doi.org/10.1016/j.jsames.2018.01.003.

Macdonald, D., Gómez-Pérez, I., Franzese, J., Spalletti, L., Lawver, L., Gahagan, L., Dalziel, I., Thomas, C., Trewin, N., and Hole, M., 2003, Mesozoic break-up of SW Gondwana: Implications for South Atlantic regional hydrocarbon potential: Marine and Petroleum Geology, v. 20, p. 287–308.

Martínez Dopico, C.I., Tohver, E., López de Luchi, M.G., Wemmer, K., Rapalini, A.E., and Cawood, P., 2016, Jurassic cooling ages in Paleozoic to early Mesozoic granitoids of northeastern Patagonia: $^{40}Ar/^{39}Ar$, ^{40}K-^{40}Ar mica and U-Pb zircon evidence: International Journal of Earth Sciences, v. 106, no. 7, p. 2343–2357, https://doi.org/10.1007/s00531-016-1430-0.

Martínez Dopico, C.I., López de Luchi, M.G., Rapalini, A.E., Wemmer, K., Fanning, C.M., and Basei, M.A.S., 2017, Emplacement and temporal constraints of the Gondwanan intrusive complexes of northern Patagonia: La Esperanza plutono-volcanic case: Tectonophysics, v. 712–713, p. 249–269, https://doi.org/10.1016/j.tecto.2017.05.015.

Max, M.D., Ghidella, M., Kovacs, L., Paterlini, M., and Valladares, J.A., 1999, Geology of the Argentine continental shelf and margin from aeromagnetic survey: Marine and Petroleum Geology, v. 16, p. 41–64, https://doi.org/10.1016/S0264-8172(98)00063-4.

Melchor, R.N., 1999, Redefinición estratigráfica de la Formación Carapacha (Pérmico), Provincia de La Pampa: Revista de la Asociación Geológica Argentina, v. 54, p. 99–108.

Muravchik, M., D'Elia, L., Bilmes, A., and Franzese, J.R., 2011, Syn-eruptive/inter-eruptive relations in the syn-rift deposits of the Precuyano Cycle, Sierra de Chacaico, Neuquén Basin, Argentina: Sedimentary Geology, v. 238, p. 132–144, https://doi.org/10.1016/j.sedgeo.2011.04.008.

Naipauer, M., and Ramos, V.A., 2016, Changes in source areas at Neuquén Basin: Mesozoic evolution and tectonic setting based on U-Pb ages on zircons, *in* Folguera, A., Naipauer, M., Sagripanti, L., Ghiglione, M., Orts, D., and Giambiagi, L., eds., Growth of the Southern Andes: Cham, Springer International Publishing, p. 33–61, https://doi.org/10.1007/978-3-319-23060-3_3.

Naipauer, M., Tunik, M., Marques, J.C., Rojas Vera, E.A., Vujovich, G.I., Pimentel, M.M., and Ramos, V.A., 2014, U-Pb detrital zircon ages of Upper Jurassic continental successions: Implications for the provenance and absolute age of the Jurassic-Cretaceous boundary in the Neuquén Basin, *in* Sepúlveda, S., Giambiagi, L., Pinto, L., Moreiras, S., Tunik, M., Hoke, G., and Farías, M., eds., Geodynamic Processes in the Andes of Central Chile and Argentina: Geological Society of London Special Publication 399, p. 131–154.

Naipauer, M., Garcia Morabito, E., Manassero, M., Valencia, V.V., and Ramos, V.A., 2018, A Provenance Analysis from the Lower Jurassic Units of the Neuquén Basin: Volcanic Arc or Intraplate Magmatic Input?, *in* Folguera, A., et al., eds., The Evolution of the Chilean-Argentinean Andes: Springer International Publishing, p. 191–222, https://doi.org/10.1007/978-3-319-67774-3_8.

Pángaro, F., and Ramos, V.A., 2012, Paleozoic crustal blocks of onshore and offshore central Argentina: New pieces of the southwestern Gondwana collage and their role in the accretion of Patagonia and the evolution of Mesozoic south Atlantic sedimentary basins: Marine and Petroleum Geology, v. 37, p. 162–183, https://doi.org/10.1016/j.marpetgeo.2012.05.010.

Pankhurst, R.J., and Rapela, C.W., 1995, Production of Jurassic rhyolite by anatexis of the lower crust of Patagonia: Earth and Planetary Science Letters, v. 134, p. 23–36, https://doi.org/10.1016/0012-821X(95)00103-J.

Pankhurst, R.J., Riley, T.R., Fanning, C.M., and Kelley, S.P., 2000, Episodic silicic volcanism in Patagonia and the Antarctic Peninsula: Chronology of magmatism associated with the break-up of Gondwana: Journal of Petrology, v. 41, p. 605–625, https://doi.org/10.1093/petrology/41.5.605.

Pankhurst, R.J., Rapela, C.W., Fanning, C.M., and Márquez, M., 2006, Gondwanide continental collision and the origin of Patagonia: Earth-Science Reviews, v. 76, p. 235–257, https://doi.org/10.1016/j.earscirev.2006.02.001.

Pankhurst, R.J., Rapela, C.W., Lopez de Luchi, M.G., Rapalini, A.E., Fanning, C.M., and Galindo, C., 2014, The Gondwana connections of northern Patagonia: Journal of the Geological Society of London, v. 171, p. 313–328, https://doi.org/10.1144/jgs2013-081.

Pavón Pivetta, C., Gregori, D., Benedini, L., Garrido, M., Strazzere, L., Geraldes, M., Santos, C.D.A., and Marcos, P., 2019, Contrasting tectonic settings in Northern Chon Aike Igneous Province of Patagonia: Subduction and mantle plume-related volcanism in the Marifil formation: International Geology Review, v. 62, no. 15, p. 1904–1930, https://doi.org/10.1080/00206814.2019.1669227.

Pujols, E.J., Leva López, J., Stockli, D.F., Rossi, V.M., and Steel, R.J., 2018, New insights into the stratigraphic and structural evolution of the middle Jurassic S. Neuquén Basin from Detrital Zircon (U-Th)/(He-Pb) and Apatite (U-Th)/He ages: Basin Research, v. 30, p. 1280–1297, https://doi.org/10.1111/bre.12304.

Pullen, A., Ibanez-Mejia, M., Gehrels, G., Ibanez-Mejia, J., and Pecha, M., 2014, What happens when n = 1000?: Creating large-n geochronological datasets with LA-ICP-MS for geologic investigations: Journal of Analytical Atomic Spectrometry, v. 29, p. 971–980, https://doi.org/10.1039/C4JA00024B.

Ramos, V.A., 1999, Las provincias geológicas del territorio argentino, *in* Caminos, R.L., ed., Geología Argentina: Segemar Anales, v. 29, p. 41–96.

Rapalini, A.E., López de Luchi, M., Tohver, E., and Cawood, P.A., 2013, The South American ancestry of the North Patagonian Massif: Geochronological evidence for an autochthonous origin?: Terra Nova, v. 25, p. 337–342, https://doi.org/10.1111/ter.12043.

Rapela, C.W., and Pankhurst, R.J., 1993, El volcanismo riolítico del noreste de la Patagonia: Un evento meso-jurásico de corta duración y origen profundo, Mendoza, Actas del XII Congreso Geológico Argentino, 4, p. 179–188.

Rapela, C.W., and Pankhurst, R.J., 2020, The continental crust of Northeastern Patagonia: Ameghiniana, v. 57, p. 480–498, https://doi.org/10.5710/AMGH.17.01.2020.3270.

Rapela, C.W., Pankhurst, R.J., Fanning, C.M., and Grecco, L.E., 2003, Basement evolution of the Sierra de la Ventana Fold Belt: New evidence for Cambrian continental rifting along the southern margin of Gondwana: Journal of the Geological Society of London, v. 160, p. 613–628.

Rapela, C.W., Pankhurst, R.J., Fanning, C.M., and Hervé, F., 2005, Pacific subduction coeval with the Karoo mantle plume: The Early Jurassic Subcordilleran belt of northwestern Patagonia: Geological Society of London Special Publication 246, p. 217–239, https://doi.org/10.1144/GSL.SP.2005.246.01.07.

Rapela, C.W., Pankhurst R.J., Casquet, C., Fanning, C.M., Baldo, E.G., González-Casado, J.M., Galindo, C., and Dahquist, J.A., 2007, The Río de la Plata craton and the assembly of SW Gondwana: Earth-Science Reviews, v. 83, p. 49–82.

Rapela, C.W., Fanning, C.M., Casquet, C., Pankhurst, R.J., Spalletti, L.A., Poiré, D., and Baldo, E.G., 2011, The Rio de la Plata craton and the adjoining Panafrican/Brasiliano terranes: Their origins and incorporation into south-west Gondwana: Gondwana Research, v. 20, p. 673–690, https://doi.org/10.1016/j.gr.2011.05.001.

Rapela, C.W., Pankhurst, R.J., Casquet, C., Dahlquist, J.A., Fanning, C.M., Baldo, E.G., Galindo, C., Alasino, P.H., Ramacciotti, C.D., Verdecchia, S.O., Murra, J.A., and Basei, M.A.S., 2018, A review of the Famatinian Ordovician magmatism in southern South America: Evidence of lithosphere reworking and continental subduction in the early proto-Andean margin of Gondwana: Earth-Science Reviews, v. 187, p. 259–285, https://doi.org/10.1016/j.earscirev.2018.10.006.

Remírez, M., Spalletti, L.A., and Isla, M.F., 2020, Petrographic, mineralogical and geochemical characterization of fine-grained rocks of the Pilmatué Member (Upper Valanginian–Lower Hauterivian) of the Neuquén Basin (Argentina): Implications for siliciclastic input, carbonate productivity and redox conditions: Journal of South American Earth Sciences, v. 102, https://doi.org/10.1016/j.jsames.2020.102663.

Riley, T.R., Millar, I.L., Watkeys, M.K., Curtis, M.L., Leat, E.T., Klausen, M.B., and Fanning, C.M., 2004, U-Pb zircon (SHRIMP) ages for the Lebombo rhyolites, South Africa: Refining the duration of Karoo volcanism: Journal of the Geological Society of London, v. 161, p. 547–550, https://doi.org/10.1144/0016-764903-181.

Sagasti, G., 2005, Hemipelagic record of orbitally-induced dilution cycles in Lower Cretaceous sediments of the Neuquén Basin, *in* Veiga, G.D., Spalletti, L.A., Howell, J.A., and Schwarz, E., eds., The Neuquén Basin: A Case Study in Sequence Stratigraphy and Basin Dynamics: Geological Society of London Special Publication 252, p. 231–250, https://doi.org/10.1144/GSL.SP.2005.252.01.11.

Sato, A.M., Llambías, E.J., Basei, M.A.S., and Leanza, H.A., 2008, The Permian Choiyoi cycle in Cordillera del Viento (Principal Cordillera, Argentina): Over 25 Ma of magmatic activity, *in* Proceedings, 6th South American Symposium on Isotope Geology, Buenos Aires, Argentina, CD-ROM.

Sato, A.M., Llambías, E.J., Basei, M.A.S., and Castro, C.E., 2015, Three stages in the Late Paleozoic to Triassic magmatism of southwestern Gondwana, and the relationships with the volcanogenic events in coeval basins: Journal of South American Earth Sciences, v. 63, p. 48–69, https://doi.org/10.1016/j.jsames.2015.07.005.

Schiuma, M., and Llambías, E.J., 2008, New ages and chemical analysis on Lower Jurassic volcanism close to the Dorsal de Huincul, Neuquén: Revista de la Asociación Geológica Argentina, v. 63, p. 644–652.

Schwarz, E., and Howell, J.A., 2005, Sedimentary evolution and depositional architecture of a Lowstand Sequence Set: The Lower Cretaceous Mulichinco Formation, Neuquén Basin, Argentina, *in* Veiga, G.D., Spalletti, L.A., Howell, J.A., and Schwarz, E., eds., The Neuquén Basin: A Case Study in Sequence Stratigraphy and Basin Dynamics: Geological Society of London Special Publication 252, p. 109–138, https://doi.org/10.1144/GSL.SP.2005.252.01.06.

Schwarz, E., Spalletti, L.A., Veiga, G.D., and Fanning, M., 2016, First U-Pb SHRIMP Age for the Pilmatué Member (Agrio Formation) of the Neuquén Basin, Argentina: Implications for the Hauterivian Lower Boundary: Cretaceous Research, v. 58, p. 223–233, https://doi.org/10.1016/j.cretres.2015.10.003.

Schwarz, E., Echevarria, C., and Veiga, G.D., 2018a, Sedimentología y estratigrafía secuencial de alta resolución de reservorios no convencionales de origen deltaico del Miembro Pilmatué (Formación Agrio, Cuenca Neuquina), *in* Santiago, M., Fantín, M., Vallejo, M.D., González Tomassini, F., Estrada, S., Marchal, D., Aguirre, H., and López, S., eds., Simposio Reservorios No Convencionales, 10° Congreso de Exploración y Desarrollo de Hidrocarburos, Mendoza, Argentina: Instituto Argentino del Petróleo, p. 363–385.

Schwarz, E., Veiga, G.D., Álvarez Trentini, G., Isla, M.F., and Spalletti, L.A., 2018b, Expanding the spectrum of shallow-marine, mixed carbonate-siliciclastic systems: Processes, facies distribution, and depositional controls of a siliciclastic-dominated example: Sedimentology, v. 65, p. 1558–1589, https://doi.org/10.1111/sed.12438.

Schwarz, E., Veiga, G.D., Echevarria, A., and Spalletti, L.A., 2019, Large-Scale Depositional and Palaeogeographic Reconstruction of the Pilmatué Member (Neuquén Basin): Understanding from the Source to the Sink: American Association of Petroleum Geologists International Convention and Exhibition, Buenos Aires, Argentina, Abstracts (digital format).

Silvestro, J., and Zubiri, M., 2008, Convergencia Oblicua: Modelo estructural alternativo para la Dorsal Neuquina (39°S), Neuquén: Revista de la Asociación Geológica Argentina, v. 63, p. 49–64.

Spalletti, L.A., 1993, An iron-bearing wave-dominated siliciclastic shelf: Facies analysis and paleogeographic implications (Silurian-Lower Devonian Sierra Grande Formation, Southern Argentina: Geological Journal, v. 28, no. 2, p. 137–148, https://doi.org/10.1002/gj.3350280204.

Spalletti, L.A., and Veiga, G.D., 2007, Variability of continental depositional systems during lowstand sedimentation: An example from the Kimmeridgian of the Neuquén Basin, Argentina: Latin American Journal of Sedimentology and Basin Analysis, v. 14, p. 85–104.

Spalletti, L.A., Arregui, C., and Veiga, G.D., 2011, La Formación Tordillo y equivalentes (Jurásico Tardío) en la Cuenca Neuquina, *in* Leanza, H.A., Arregui, C., Carbone, O., Danielli, J.C., and Vallés, J.M., eds., Geología y Recursos Naturales de la Provincia del Neuquén, 18° Congreso Geológico Argentino, Argentina: Asociación Geológica Argentina, p. 99–111.

Strazzere, L., Gregori, D.A., Benedini, L., Marcos, P., and Barros, M., 2017, Edad y petrología del Complejo Volcánico Marifil en la Sierra de Pailemán, Comarca Nordpatagónica, Río Negro, Argentina, in Proceedings, 20 Congreso Geológico Argentino, Argentina, p. 145–150.

Thomas, W.A., Gehrels, G.E., Sundell, K.E., Greb, S.F., Finzel, E.S., Clark, R.J., Malone, D.H., Hampton, B.A., and Romero, M.C., 2020, Detrital zircons and sediment dispersal in the eastern Midcontinent of North America: Geosphere, v. 16, p. 817–843, https://doi.org/10.1130/GES02152.1.

Tickyj, H., Tomezzoli, R., Chemale, F., Jr., and Rapalini, A., 2010, Litología y edad de las volcanitas del cerro Centinela, provincia de La Pampa: 10th Congreso de Mineralogía y Metalogénesis, Universidad Nacional de Río Cuarto, Argentina, Abstracts, p. 375–376.

Tohver, E., Cawood, P.A., Rossello, E., López de Luchi, M.G., Rapalini, A., and Jourdan, F., 2008, New SHRIMP U–Pb and $^{40}Ar/^{39}Ar$ constraints on the crustal stabilization of southern South America, from the margin of the Rio de Plata (Sierra de Ventana) craton to northern Patagonia: Abstract T23C-2052 presented at 2008 Fall Meeting, AGU, San Francisco, California, 15–19 December.

Tunik, M., Folguera, A., Naipauer, M., Pimentel, M.M., and Ramos, V.A., 2010, Early uplift and orogenic deformation in the Neuquén Basin: Constraints on the Andean uplift from U-Pb and Hf isotopic data of detrital zircons: Tectonophysics, v. 489, p. 258–273, https://doi.org/10.1016/j.tecto.2010.04.017.

Uliana, M.A., Dellapé, D.A., and Pando, G.A., 1977, Análisis estratigráfico y evaluación del potencial petrolífero de las formaciones Mulichinco, Chachao y Agrio (Cretácico

Inferior de las Provincias de Neuquén y Mendoza): Petrotecnia, v. 31, p. 31–46.
Uriz, N.J., Cingolani, C.A., Chemale, F., Jr., Macambira, M.B., and Armstrong, R., 2011, Isotopic studies on detrital zircons of Silurian–Devonian siliciclastic sequences from Argentinean North Patagonia and Sierra de la Ventana regions: Comparative provenance: International Journal of Earth Sciences, v. 100, p. 571–589, https://doi.org/10.1007/s00531-010-0597-z.
Van Lente, B., 2004, Chemostratigraphic trends and provenance of the Permian Tanqua and Laingsburg depocentres, South Western Karoo Basin, South Africa [Ph.D. thesis]: Stellenbosch, University of Stellenbosch, 339 p.
Veiga, G.D., and Schwarz, E., 2016, Facies characterization and sequential evolution of an ancient offshore dunefield in a semi-enclosed sea: Neuquén Basin, Argentina: Geo-Marine Letters, v. 37, p. 411–426, https://doi.org/10.1007/s00367-016-0467-1.
Veiga, G.D., and Vergani, G.D., 2011, El Miembro Troncoso Inferior de la Formación Huitrín (Cretácico Temprano), *in* Leanza, H.A., Arregui, C., Carbone, O., Danielli, J.C., and Vallés, J.M., eds., Geología y Recursos Naturales de la Provincia del Neuquén, 18° Congreso Geológico Argentino, Argentina; Asociación Geológica Argentina, p. 181–188.
Veiga, G.D., Howell, J.A., and Strömbäck, A., 2005, Anatomy of a mixed marine/non-marine lowstand wedge in a ramp setting. The record of a Barremian/Aptian complex relative sea-level fall in Central Neuquén Basin, Argentina, *in* Veiga, G.D., Spalletti, L.A., Howell, J.A., and Schwarz, E., eds., The Neuquén Basin: A Case Study in Sequence Stratigraphy and Basin Dynamics: Geological Society of London Special Publication 252, p. 139–162, https://doi.org/10.1144/GSL.SP.2005.252.01.07.
Veiga, G.D., Spalletti, L.A., and Flint, S.S., 2007, Anatomy of a fluvial lowstand wedge: The Avilé Member of the Agrio Formation (Hauterivian) in central Neuquén Basin (northwest Neuquén province), Argentina, *in* Nichols, G., Williams, E., and Paola, C., eds., Sedimentary Environments, Processes and Basins: A Tribute to Peter Friend: IAS Special Publication 38, p. 341–365, https://doi.org/10.1002/9781444304411.ch16.
Veiga, G.D., Spalletti, L.A., and Schwarz, E., 2011, El Miembro Avilé de la Formación Agrio (Cretácico Temprano), *in* Leanza, H.A., Arregui, C., Carbone, O., Danielli, J.C., and Vallés, J.M., eds., Geología y Recursos Naturales de la Provincia del Neuquén, 18° Congreso Geológico Argentino, Argentina: Asociación Geológica Argentina, p. 161–173.
Veiga, G.D., Schwarz, E., and Finzel, E., 2019, Reconstructing the large-scale sediment delivery systems during the Early Cretaceous in the Neuquén Basin (Argentina), 35th International Meeting of Sedimentology, Roma, Italia, Abstracts (digital format).
Vergani, G.D., Tankard, A.J., Belotti, H.J., and Welsink, H.J., 1995, Tectonic evolution and paleogeography of the Neuquén Basin, Argentina, *in* Tankard, A.J., Suarez Soruco, R., and Welsink, H.J., eds., Petroleum Basins of South America: American Association of Petroleum Geologists Memoir 62, p. 383–402.
Weaver, V., 1931, Palaeontology of the Jurassic and Cretaceous of West Central Argentina: University of Washington Memoir 1, 595 p.
Will, T.M., and Frimmel, H.E., 2018, Where does a continent prefer to break up?: Some lessons from the South Atlantic margins: Gondwana Research, v. 53, p. 9–19, https://doi.org/10.1016/j.gr.2017.04.014.
Zappettini, E.O., Lagorio, S.L., Dalponte, M., Santos, J.O., and Belousova, E., 2019, Evidencias de magmatismo Precuyano (Pliensbachiano-Toarciano) en el norte de la Cordillera del Viento, provincia del Neuquén: Caracterización geoquímica, isotópica e implicancias tectónicas: Revista de la Asociación Geológica Argentina, v. 75, p. 533–558.
Zavala, C., and Ponce, J., 2011, La Formación Rayoso (Cretácico Temprano) en la Cuenca Neuquina, *in* Leanza, H.A., Arregui, C., Carbone, O., Danielli, J.C., and Vallés, J.M., eds., Geología y Recursos Naturales de la Provincia del Neuquén, 18° Congreso Geológico Argentino, Argentina: Asociación Geológica Argentina, p. 205–222.
Zavala, C., Ponce, J.J., Arcuri, M., Drittanti, D., Freije, H., and Asensio, M., 2006, Ancient lacustrine hyperpycnites: A depositional model from a case study in the Rayoso Formation (Cretaceous) of west-central Argentina: Journal of Sedimentary Research, v. 76, p. 41–59, https://doi.org/10.2110/jsr.2006.12.